# Modelling the Compliance of Swelling Clay Sealing Systems: In-Floor Borehole and Horizontal Borehole Numerical Simulations

**NWMO TR-2008-13** **November 2008**

**N. A. Chandler**

Independent Engineering Consultant

nwmo
NUCLEAR WASTE MANAGEMENT ORGANIZATION
SOCIÉTÉ DE GESTION DES DÉCHETS NUCLÉAIRES

**Nuclear Waste Management Organization**
22 St. Clair Avenue East, 6th Floor
Toronto, Ontario
M4T 2S3
Canada

Tel: 416-934-9814
Web: www.nwmo.ca

# Modelling the Compliance of Swelling Clay Sealing Systems: In-Floor Borehole and Horizontal Borehole Numerical Simulations

**NWMO TR-2008-13**

November 2008

**N. A. Chandler**

Independent Engineering Consultant

## ABSTRACT

**Title:** **Modelling the Compliance of Swelling Clay Sealing Systems: In-Floor Borehole and Horizontal Borehole Numerical Simulations**
**Report No.:** **NWMO TR-2008-13**
**Author(s):** N. A. Chandler
**Company:** Independent Engineering Consultant
**Date:** November 2008

**Abstract**
Compliance modelling can provide insight into density changes of swelling clay materials upon saturation. For example, the higher the dry density of bentonite after saturation at the surface of a used-fuel container, the lower is the potential for microbially-influenced corrosion of the container. This report describes a numerical analysis that considers the relative compliance of the swelling and non-swelling clay materials upon full saturation. The Fast Lagrangian Analysis of Continua (FLAC) analysis software code was used, and non-linear elastic properties were input into the model. The non-linear properties were based on the relationship between mean stress, or swelling pressure, and Effective Montmorillonite Dry Density (EMDD). Different density versus mean stress relationships were used for different pore water salinities and also to represent different mean stress versus volume strain paths during swelling expansion (unloading) and compression (loading).

Two different container placement options for a deep geological repository for used nuclear fuel were simulated: a horizontal borehole option, and a vertical in-floor borehole option. In both options, highly compacted bentonite (HCB) was placed adjacent to a material comprised of bentonite pellets or granules. Upon saturation, the expansion of the HCB resulted in a reduction of its dry density concurrent with a compression of the adjacent bentonite pellet materials. Compliance modelling provides a tool for assessing the required as-placed densities of both the HCB and bentonite pellets in order to achieve specific targets for long-term dry densities. Results are presented relative to a minimum dry density of 1.4 $Mg/m^3$ for the bentonite adjacent to the used-fuel container. 1.4 $Mg/m^3$ represents the dry density of bentonite above which research indicates microbe culturability to be at or below background levels.

## TABLE OF CONTENTS

## LIST OF TABLES

**Page**



## LIST OF FIGURES

**Page**

## 1. INTRODUCTION

The inclusion of 100% bentonite clay adjacent to a copper and steel used-fuel container is an integral component of many proposed designs for containment and isolation of used nuclear fuel in a deep geological repository. The small pore spaces in highly compacted bentonite (HCB) combined with low water activity in these pore spaces result in very low microbial activity. Water activity is defined as the ratio of partial vapour pressure of the pore fluid to the partial vapour pressure of pure water. Lowering the microbial activity will be beneficial for minimising the potential for microbially-influenced corrosion of used-fuel containers. Previously, Maak and Stroes-Gascoyne (2008) and Stroes-Gascoyne and Hamon (2008) document experimental evidence showing that higher bentonite densities result in reduced microbial activity within the material. Maak and Stroes-Gascoyne (2008) stated that an HCB dry density greater than 1.6 $Mg/m^3$ would be sufficient to reduce the water activity in the HCB is less than 0.96, which is considered to be the lower limit for microbial activity. Additional test results presented by Stroes-Gascoyne and Hamon (2008) indicated that the dry density of HCB required to keep microbial culturability at or below background levels could be as low as 1.4 $Mg/m^3$, pending confirmation through pore size analysis.

Potential used-fuel container placement room configurations often include high-density pre-compacted bentonite blocks adjacent to construction gaps filled with bentonite pellets. The bentonite blocks are formed by static compression to dry densities of between 1.7 and 1.8 $Mg/m^3$. The individual bentonite granules or pellets have very high densities (up to 2.2 $Mg/m^3$), however, they collectively form a material that initially has large pore spaces between the pellets with an overall density that is less than that of the HCB. Saturation of both materials in a confined tunnel results in volumetric expansion (swelling) of the HCB blocks concurrent with compression of the lower-density pellet-filled regions. During the transient saturation period, the dry density of the pellet material increases, while the dry density of the HCB blocks decreases. To minimise the potential for microbially-influenced corrosion, it would be advantageous if the final dry density of the material in contact with the container, whether it's HCB or bentonite pellets, was as high as possible.

An approximate method for estimating the final dry density of the bentonite within the container placement borehole would be to assume that the density would ultimately equilibrate throughout. Kjartanson et al. (2003) suggested that a limiting case for density calculations would be for all the clay materials to eventually become a homogeneous mass. In this limiting case, all the materials would have the same swelling pressure and would have the same Effective Montmorillonite Dry Density[1]. The average density computed in this way would then be used to evaluate the potential microbial activity in the saturated material. Although the calculation method used by Kjartanson et al. (2003) is useful, it could be misleading. There is no experimental evidence to support the assumption of complete homogenization of the different materials. This would be analogous to the equalization of pressures for two fluids in contact, which is not an accurate representation of geotechnical materials. From a mechanical perspective, this could only be achieved if the compacted bentonite had an elastic Shear Modulus equal to zero. The density at the container surface calculated using this method would be lower than the actual density if HCB was adjacent to the container, or higher than actual if

[1] Effective Montmorillonite Dry Density (EMDD) is the dry density of the active swelling component of bentonite (montmorillonite) with the non-active material constituents treated as inert filler. The calculation of EMDD is described in Section 3.1.

the bentonite pellet material was placed next to the container. The expansion of the HCB and the corresponding compression of the bentonite pellets will be dependent upon the relative compliance of the two materials.

This report describes the saturated sealing-system compliance modelling for two different proposed sealing system configurations. The first numerical model simulates the compliance of the bentonite materials in a horizontal placement design option in a large-diameter (2.5 m) borehole, similar to that proposed by NAGRA (2002) and evaluated by Baumgartner (2005). The second compliance model simulates the vertical in-floor borehole placement geometry described by RWE NUKEM (2003).

## 2. COMPLIANCE MODELLING

Compliance modelling refers to the computation of densities of clay-based sealing materials following the concurrent expansion of some swelling clays, compression of other swelling or non-swelling clays, and the collapse of initially air-filled construction gaps. The compliance model computes the material densities that would ultimately be achieved long after saturation is complete. The model does not attempt to compute the properties of the materials during the transient stage of partial saturation nor the time-dependent swelling of the saturated material. Although the stresses within the material is computed by the compliance model, it is not intended for use in evaluation of the mechanical stability, but rather as a tool to estimate the final material densities. The three basic requirements for successful compliance modelling are listed below.

1. There must be at least two different clay-based materials present, of which one must have a component of swelling clay. The only exception is that compliance modelling could be performed if there is only one swelling clay material and an initially open gap.
2. There must be a known relationship between density and mean stress for the swelling clays.
3. The swelling clays cannot behave as a fluid. That is, the material is allowed to have different stresses in different directions in its equilibrium state. This condition is satisfied if the materials have a Poisson's Ratio less than 0.5 or a Shear Modulus greater than zero.

The assumptions inherent in the compliance modelling, as well as important attributes and limitations, are listed below.

- The materials are assumed to become saturated relatively quickly and the stress or strain history prior to saturation is ignored.
- The current compliance model cannot incorporate stress-strain modelling of materials that are unsaturated. In reality, however, an unsaturated material will compress and increase in density as the outer regions become saturated and expand. The effect that this has on the final density has not been analysed.
- Mean stress (the average of the three principal stresses, $\sigma_1$, $\sigma_2$, $\sigma_3$) is considered as being equivalent to swelling pressure, $P_s$.

$$P_s = (\sigma_1 + \sigma_2 + \sigma_3)/3 \qquad [1]$$

- Swelling pressure is only dependent upon the Effective Montmorillonite Dry Density (EMDD) and the same EMDD versus mean stress relationship applies to all swelling clay materials

(i.e. HCB, bentonite pellets, light backfill, and compacted sand-bentonite buffer). The exception is for stiff materials having very low EMDD, and hence very low swelling pressures, such as dense backfill (DBF). DBF has been assumed to compress elastically under to externally applied loads, and the mean stress that can be sustained by the DBF is can be greater than its swelling pressure.

- The EMDD versus mean stress relationship depends only on salinity, and the salinity is assumed to be homogeneous throughout the saturated placement room.
- All the sealing materials have shear resistance and do not behave as a fluid with equal pressure in all directions. The Shear Modulus ($G$) is assumed to be proportional to the Bulk Modulus ($K$), using $G = \alpha K$ where $\alpha$ is dependent upon the assumed value of Poisson's Ratio. (See Section 3.2 for determination of $\alpha$.) For a given material, Poisson's Ratio is taken to be constant at all densities.
- To simulate hysteresis, different mean stress versus EMDD relationships can be used for those materials that are swelling (expanding) and those materials that are compressing.
- Gravitational loads due to the materials or containers can potentially contribute to a small decrease in swelling expansion. However, this effect is sufficiently small that it can be ignored (Section 4.3).
- Shear failure is not modelled and plastic strain of failed material is not considered. All strains are calculated using non-linear elastic relationships.

The software used in the analysis was the Fast Lagrangian Analysis of Continua (FLAC)[2]. Instantaneous saturation was simulated by assigning all materials in the model an internal compressive stress equal to the swelling pressure calculated using the as-placed EMDD. In applying this model it was implied that the final saturated state of the material was independent of its stress-strain history. This is an acceptable conclusion for elastic materials, and all materials were simulated using elastic properties. However, the compliance of an unsaturated material will be different from that of a saturated material at the same dry density, and this difference could affect the final computed material response. No attempt has been made to model gradual wetting. There is also insufficient experimental data available to develop a mechanical model for an unsaturated swelling clay of varying moisture content.

Two model verification problems are summarised in Appendix A.

## 3. MATERIAL PROPERTIES REQUIRED FOR THE COMPLIANCE MODEL

### 3.1 Swelling Pressure and EMDD

Baumgartner (2006) provided relationships between swelling pressure and Effective Montmorillonite Dry Density (EMDD) for swelling clay-based materials having pore fluids with different salinities. EMDD is defined as the dry mass of montmorillonite, which is the active component of swelling clay, divided by the volume of the air- or water-filled voids plus the volume of the montmorillonite. Baumgartner (2006) provides the following equation for calculation of EMDD.

[2] The Fast Lagrangian Analysis of Continua is a stress, displacement, temperature and pore pressure analysis software code commercially available from Itasca Consulting Group Inc., 111 Third Avenue South, Suite 450 Minneapolis, MN 55401.

$$EMDD = \frac{f_m f_c \rho_d}{\left[1 - \frac{(1-f_c)\rho_d}{G_s \rho_w} - \frac{(1-f_m) f_c \rho_d}{G_n \rho_w}\right]} \quad . \qquad [2]$$

The term $f_c$ represents the clay fraction, $f_m$ is the montmorillonite fraction in the clay, $G_s$ and $G_n$ are the specific gravities of the sand and the non-swelling clay, $\rho_w$ is the density of water and $\rho_d$ is the dry density of the composite material. The calculation of EMDD allows materials with different compositions of aggregate, non-swelling clay and swelling clay to be compared. The flowing five equations describe the relationship between EMDD (in Mg/m$^3$) and swelling pressure ($P_s$ in MPa) for swelling clays permeated with pore fluids having different salinities (Baumgartner, 2006). Salinity is expressed in terms of Total Dissolved Solids (g/L).

0 g/L $\quad P_s = 1\times10^{-2}\, e^{4.58EMDD}$ [3a]

35-60 g/L $\quad P_s = 4\times10^{-3}\, e^{5.0EMDD}$ [3b]

100 g/L $\quad P_s = 2\times10^{-3}\, e^{5.3EMDD}$ [3c]

175 g/L $\quad P_s = 6\times10^{-4}\, e^{5.83EMDD}$ [3d]

350 g/L $\quad P_s = 2.3\times10^{-4}\, e^{6.26EMDD}$ [3e]

These relationships are presumed to be valid for materials that are comprised of 50% to 100% bentonite. The relationships and the data on which it was based are illustrated in Figure 1.

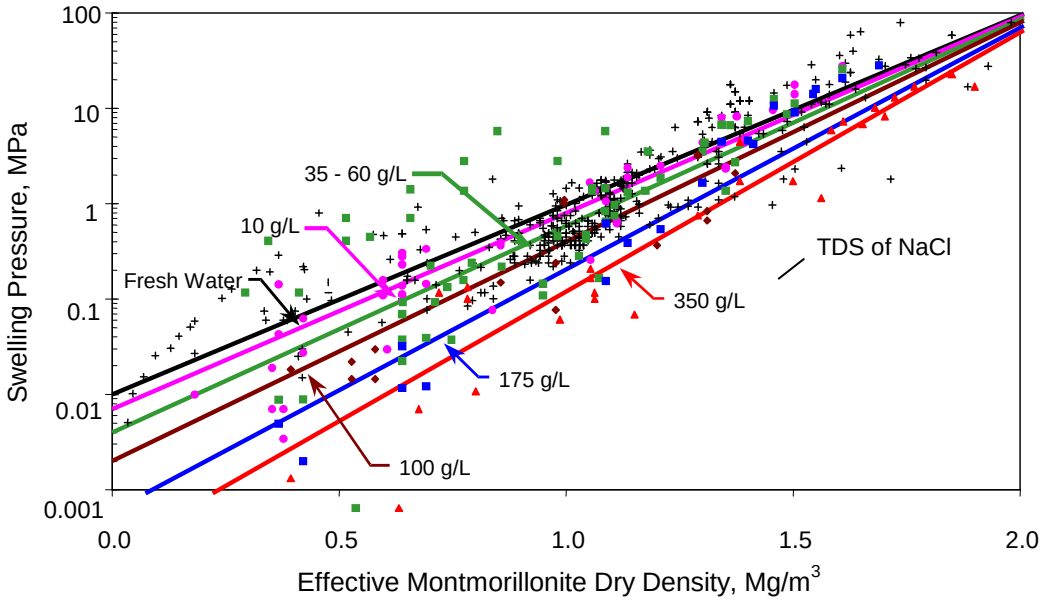


**Figure 1: Swelling Pressure as a Function of Effective Montmorillonite Dry Density and Salinity.**

### 3.2 Bulk Modulus and Shear Modulus

The compliance model requires the Bulk Modulus, *K*, as input. In theory, the change in mean stress, or swelling pressure ($\Delta P_s$) can be calculated using

$$\Delta P_s = K \varepsilon_v \,, \qquad [4]$$

where $\varepsilon_v$ is the volume strain ($\varepsilon_v = \Delta V / V$). The Bulk Modulus itself is not constant but is dependent upon material density, or volume strain. The value of *K* is equivalent to the slope of the mean stress versus volume strain plot shown in Figure 2, which increases with increasing compressive strain. The following equation for Bulk Modulus as a function of EMDD was derived by expressing EMDD in terms of volume strain, substituting the expression into equations [3a-e] and then finding the derivative with respect to volume strain to obtain the slope of the curve on the right side of Figure 2.

$$K = C_1 P_s \frac{EMDD^2}{f_m f_c \rho_d} \qquad [5]$$

where $P_s$ is swelling pressure as defined by [3a-e], and $C_1$ depends only upon salinity (i.e., upon the coefficients in the EMDD term in equations [3a-e] ). The value of $C_1$ is 4.58, 5.0, 5.3, 5.83 and 6.26 (the units are $m^3/Mg$) for fresh water, 35 to 60 g/L, 100 g/L, 175 g/L and 300 g/L salinity, respectively. A plot of Bulk Modulus versus volume strain for each material under fresh water conditions is provided in Figure 3.

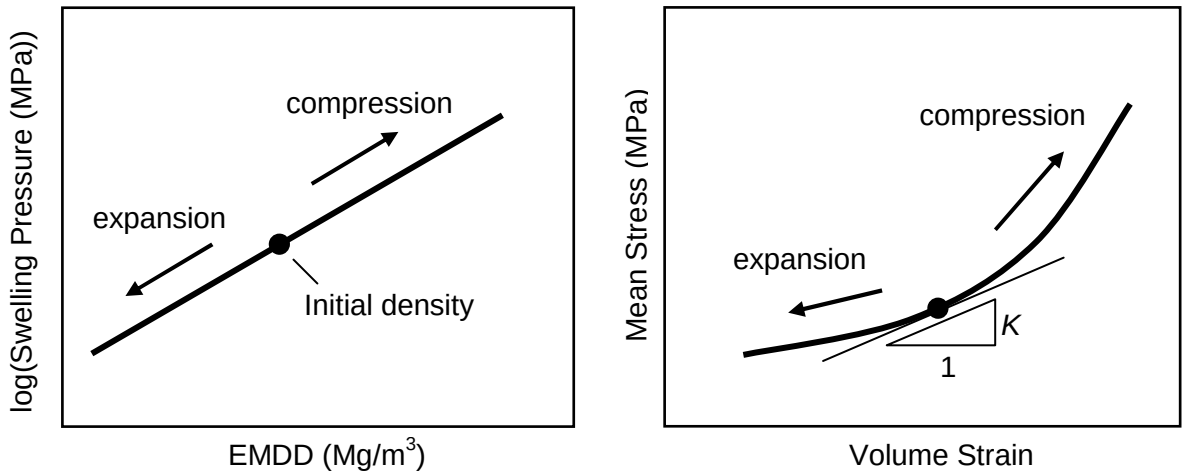


**Figure 2: Simplified Illustration of Nonlinear Elastic Material Behaviour Model**

The model also requires the Shear Modulus, *G*, as input. The Shear Modulus defines the change in shear stress in response to a change in shear strain (i.e. the distortion from its original shape). The Shear Modulus is assumed to be proportional to the Bulk Modulus, *K*. Assuming that the Poisson's Ratio, $\nu$, of the material is constant at all densities, then

$$G = 3\frac{(1-2\nu)}{(2+2\nu)}K \qquad [6]$$

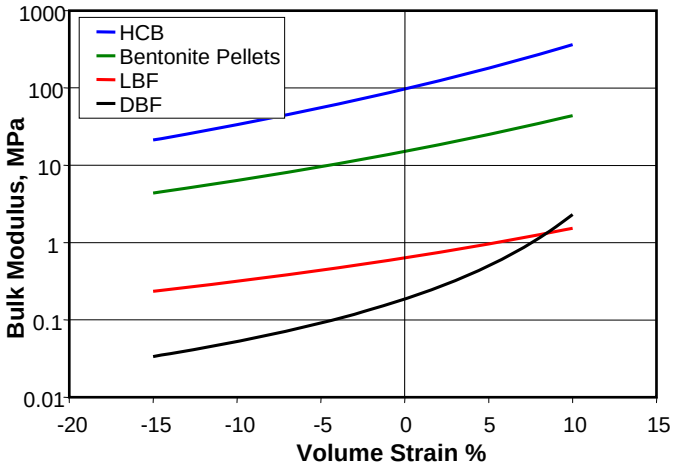


**Figure 3: Bulk Modulus as a Function of Volume Strain for each Material under Fresh Water Conditions.**

Back analyses of laboratory compliance tests have suggested that a Poisson's Ratio of about 0.4 is appropriate for compliance modelling for any saturated clay-based swelling material. The compliance model updates the dry density, $\rho_d$, and EMDD of the swelling clay materials with computed changes in volume strain using equations [7] and [8] below.

$$\rho_d = \frac{\rho_{d0}}{1-\varepsilon_v} \qquad [7]$$

$$EMDD = \frac{\rho_d f_m f_c}{\left\{1-\frac{\rho_d}{\rho_w}\left[\frac{(1-f_c)}{G_s}+\frac{(1-f_m)f_c}{G_n}\right]\right\}} \qquad [8]$$

### 3.3 Material Composition and Initial Density

Two clay-based materials, HCB and bentonite pellets, are included in the horizontal placement design option studied, while four materials are required for the in-floor borehole placement model. The materials required for the in-floor borehole model include highly compacted bentonite (HCB), bentonite pellets, dense backfill (DBF) and light backfill (LBF). However, only the HCB and bentonite pellets are found within the in-floor borehole, while the DBF and LBF are in the tunnel above the borehole. The compositions of the four materials are summarised in Table 1.

Bentonite can be compressed into large blocks having a dry density between 1.7 and 1.8 Mg/m$^3$. Smaller individual bentonite pellets can be compressed to a greater density of 2.2 Mg/m$^3$. The challenge is to compact the pellets closely together to achieve a high overall density. Weber and Plötze (2007) were able to consistently achieve dry density of 1.45 Mg/m$^3$ using pellets, however, they did demonstrate that a density of 1.5 Mg/m$^3$ was possible. Kjartanson et al. (2005) were able to achieve 1.4 Mg/m$^3$ in their study. These studies suggest that carefully placed pellets will have a dry density in the range of 1.4 to 1.5 Mg/m$^3$. The data presented in Table 1 for DBF and LBF are based on the as-placed material dry densities provided by Hobbs et al. (2005).

**Table 1: Compositions, Placement Densities and Swelling Pressures of Emplacement Room Clay-Based Materials**

| | HCB | Bentonite Pellets (Gap Fill) | DBF | LBF |
|---|---|---|---|---|
| Clay % of total mass (*fc*) | 100 | 100 | 30 | 50 |
| % of clay that is montmorillonite (*fm*) | 75 | 75 | 12.5[3] | 75 |
| Sand or granite aggregate % by mass | 0 | 0 | 70 | 50 |
| As-placed dry density ($Mg/m^3$) | 1.7 to 1.8 | 1.4 to 1.5 | 2.12 | 1.26 |
| EMDD ($Mg/m^3$)* | 1.52 to 1.63 | 1.21 to 1.31 | 0.35 | 0.66 |
| Fresh water swelling pressure (MPa)** | 10.5 to 17.2 | 2.6 to 4.0 | 0.05 | 0.20 |
| Saturated Poisson's Ratio | 0.4 | 0.4 | 0.3 | 0.4 |

* calculated based on $G_s = G_n = 2.65$ for the specific gravity of non-swelling clay and sand or granite aggregate.
** calculated using the EMDD and equation 3a.

### 3.4 Dense Backfill

For this analysis, dense backfill (DBF) was considered to have sufficiently low montmorillonite content that it was not a swelling clay material (i.e. the Bulk Modulus was not defined by [3a-e] and [5]). A stiff linear-elastic Young's Modulus of 26 MPa was selected for DBF. This modulus value was in keeping with the material's mostly granite aggregate composition and high dry density. If the material had been modelled as a swelling clay, it's very low initial EMDD and swelling pressure would have given the DBF an unreasonably high compressibility. According to equation [5] the initial Bulk Modulus would have been only 0.3 MPa. The slightly lower Poisson's Ratio of 0.3 relative to the other materials reflects a slightly greater resistance to shear distortion than if its properties were defined based on swelling alone. DBF is only located in the tunnel above the in-floor placement borehole, and is not included within the horizontal placement numerical model.

### 3.5 Loading – Unloading Hysteresis

Baumgartner et al. (2008) and Priyanto et al. (2008) document the results from a series of long-term consolidation tests on swelling clays. These tests were performed with load increments that had sufficiently long durations such that the applied load versus EMDD relationship would be indicative of the material's swelling behaviour. Upon completion of the incremental loading, the tests were then incrementally unloaded. Loading and unloading did not follow the same path on a plot of stress versus density (or EMDD) indicating a hysteresis effect. A plot of applied stress versus EMDD for HCB for a single test carried out under fresh water conditions is provided in Figure 4. A compilation of data from four tests showing loading and unloading HCB data under fresh water conditions is provided in Figure 5. Since lateral stress is not measured in a consolidation test, the swelling pressure or mean stress is taken to be equivalent to the applied vertical stress for the purpose of developing a relationship for use in this numerical analysis.

[3] This value of *fm* does not consider the potential for montmorillonite in the 'lake clay', which makes up 25% of the total mass.

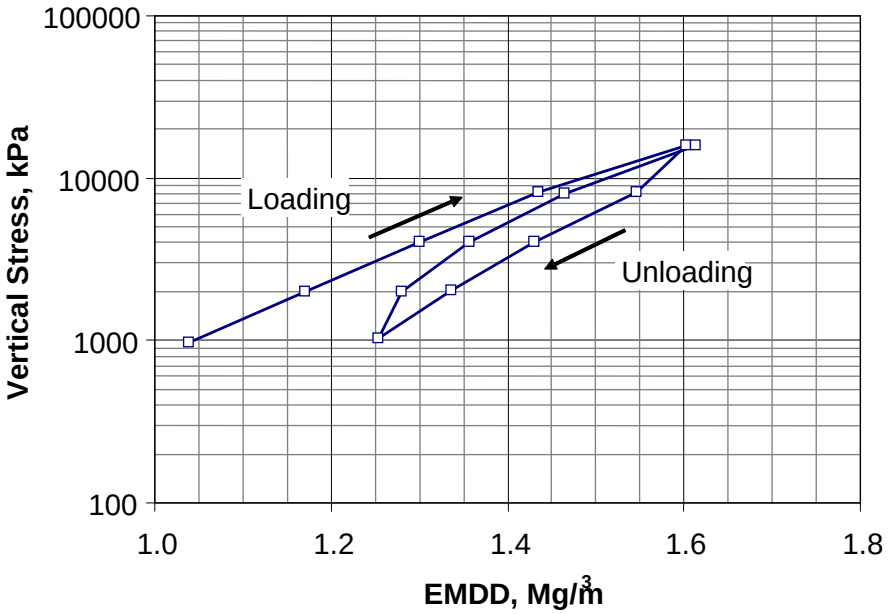


**Figure 4: Applied Vertical Stress versus EMDD from One Consolidation Test on HCB (data from Baumgartner et al. 2008).**

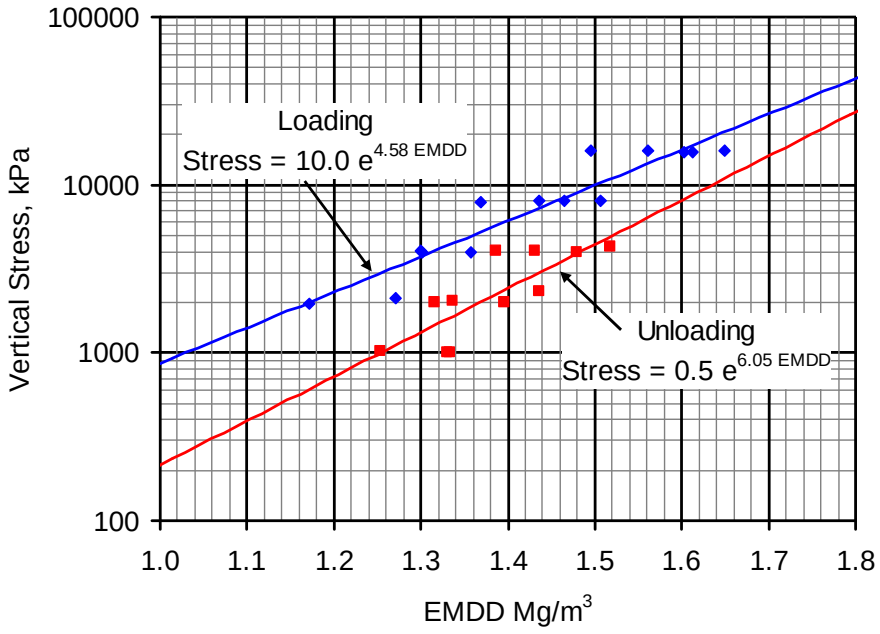


**Figure 5: Different Relationships for Vertical Stress as a Function of EMDD for HCB based on Consolidation Test Data from Baumgartner et al. 2008 and Priyanto et al. 2008.**

The loading data in Figure 5 follow the previously defined relationship for mean stress as a function of EMDD under fresh water conditions ([3a]). The equation for mean stress versus EMDD for the unloading data is provided in Figure 5, and is rewritten below.

$$P_s = 5 \times 10^{-4} e^{6.05 EMDD} \quad [9]$$

The equation is the best fit to data from only four tests that exhibit a fair amount of scatter. Equation [9] can be used as an estimate of the unloading behaviour in the compliance analyses. The data from the four tests also only cover a range of EMDD that is representative of the HCB blocks and not of the as-placed bentonite pellets. However, in this analysis, only the HCB will experience unloading as it expands. For fresh water conditions, unloading due to expansion of HCB blocks can be represented using [9], while the compression of bentonite pellets and LBF can be represented by [3a]. Although Baumgartner et al. (2008) and Priyanto et al. (2008) performed additional consolidation tests using saline water the results are too preliminary to establish a definitive mean stress versus EMDD relationship during unloading for any case other than for fresh water.

Owing to the preliminary nature of the data presented in Figure 5, the analyses were performed both with and without the use of different loading and unloading relationships.

### 3.6 Initial Stress

The approach used to numerically implement the swelling pressure in the compliance model was to impose an internal initial hydrostatic compressive stress ($\sigma_{xx} = \sigma_{yy} = \sigma_{zz}$) equal to the swelling pressure. The initial stress was dependent upon the material's as-placed EMDD and was calculated using [3a-e]. Higher density materials would have a higher initial internal compressive stress than lower density materials. The stress inequality would result in expansion of the high density materials and compression of the low density materials.

### 3.7 Concrete, Rock and the Container

The container provided a rigid incompressible inner boundary, while the rock and concrete surfaces provided rigid incompressible outer boundaries. The container was considered to be incompressible but was allowed to displace upwards or downwards with the expansion and compression of adjacent clay materials. In cases where the elastic properties of concrete, rock or the container were required as input into the software, an arbitrarily high elastic Young's Modulus was used resulting in insignificant displacements relative to the displacements in the clay.

## 4. HORIZONTAL PLACEMENT MODEL

### 4.1 Geometry and Boundary Conditions

The geometry of the horizontal placement option used in this analysis is illustrated in Figure 6. The container rests on a pedestal of HCB blocks with the remainder of the 2.5 m diameter tunnel filled with bentonite pellets. Upon saturation, the HCB pedestal will expand with a concurrent compression of the adjacent bentonite pellets. Conceivably, the HCB will also push the container upwards, thus compressing the bentonite pellet material above the container. For this reason, it was important to have an incompressible and free-floating container in the numerical simulation.

Outward displacement was prevented at the outer boundaries representing the rock surface, although shear displacement along both the container surface and the rock surface was allowed. For this model, both surfaces were modelled as being smooth and frictionless. An interface friction angle could have been set to non-zero values, however, varying the friction angle would have added another layer of complexity in the model with potentially little influence on the final results. The smooth interface with shear displacement allowed was more representative of the actual response than a rigidly fixed interface. The FLAC numerical grid is illustrated in Figure 7. The lack of radial symmetry does not lend itself to an analysis using axisymmetry. The only analysis possible was through a cross-section representing the central portion of the container and surrounding bentonite sealing system.

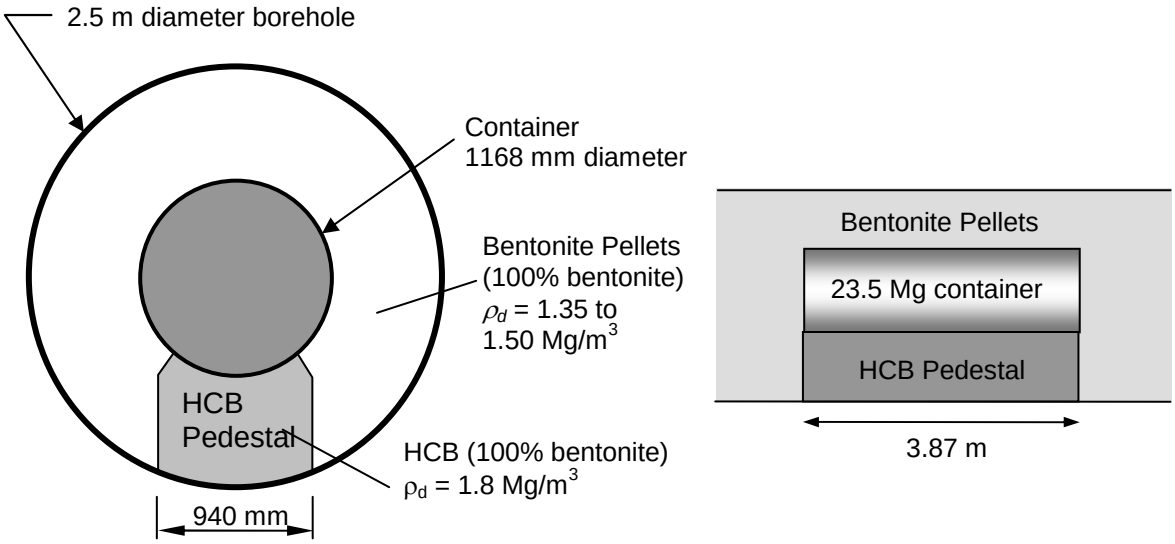


**Figure 6: Geometry of the Horizontal Canister Placement Option.**

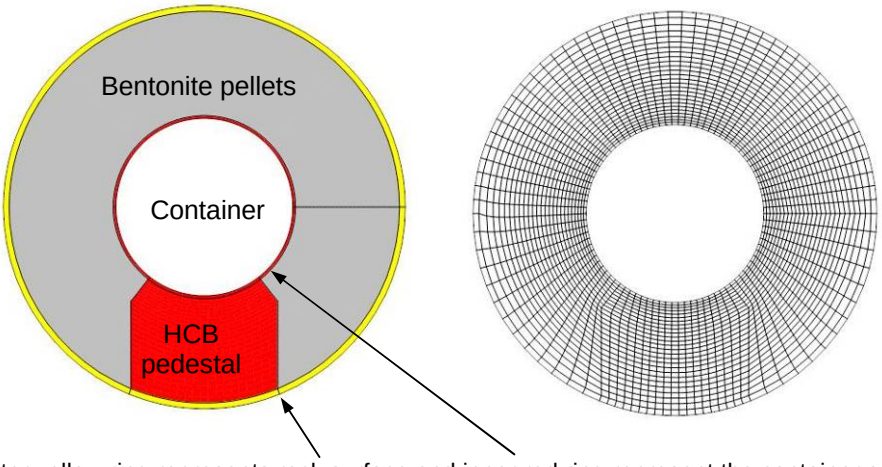


Outer yellow ring represents rock surface and inner red ring represent the container surface.

**Figure 7: Configuration of the Materials (left) and Grid (right).**

### 4.2 Results

The following are possible output quantities computed by the numerical compliance model:

- dry density
- EMDD
- displacement
- mean stress (swelling pressure)
- volume strain

Sample output plots are provided in Figure 8 (displacement and mean stress), Figure 9 (dry density) and Figure 10 (EMDD) as illustrative examples of the output that is typical of the results. The model was run using 5 different salinity conditions [Equations 3a-e] and four different initial pellet dry densities (1.35, 1.40, 1.45 and 1.50 Mg/m$^3$). Consequently, there were twenty sets of results and it would not be practical to present all contour plots for all simulations. The HCB pedestal density was 1.80 Mg/m$^3$ for all simulations.

Figure 8 shows displacement vectors and mean stress contours for the fresh water case with initial bentonite pellet placement dry density of 1.40 Mg/m$^3$. The illustration shows the expansion of the HCB pedestal and the compression of the adjacent region of pellets. There was virtually no upward movement of the canister due to HCB swelling and the dry density above the canister is essentially unchanged from as-placed conditions (Figure 9). The detail above the container in Figure 9 indicates how little the density increased above the initial density of 1.40 Mg/m$^3$ in this region. Figure 10 provides contour plots of EMDD in the placement room cross-section.

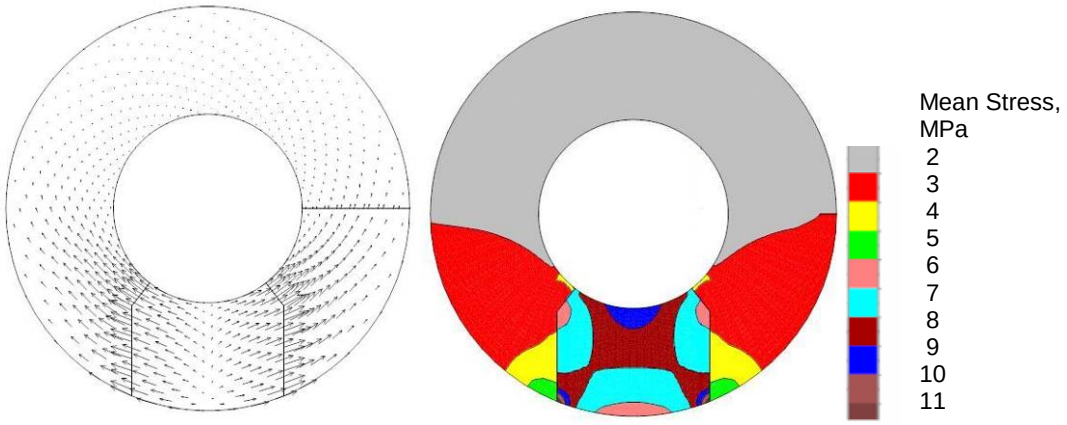


**Figure 8: Displacement Vectors (left) and Mean Stress Contours (right) for the Case of Initial Pellet Density of 1.40 Mg/m$^3$ and Fresh Water.**

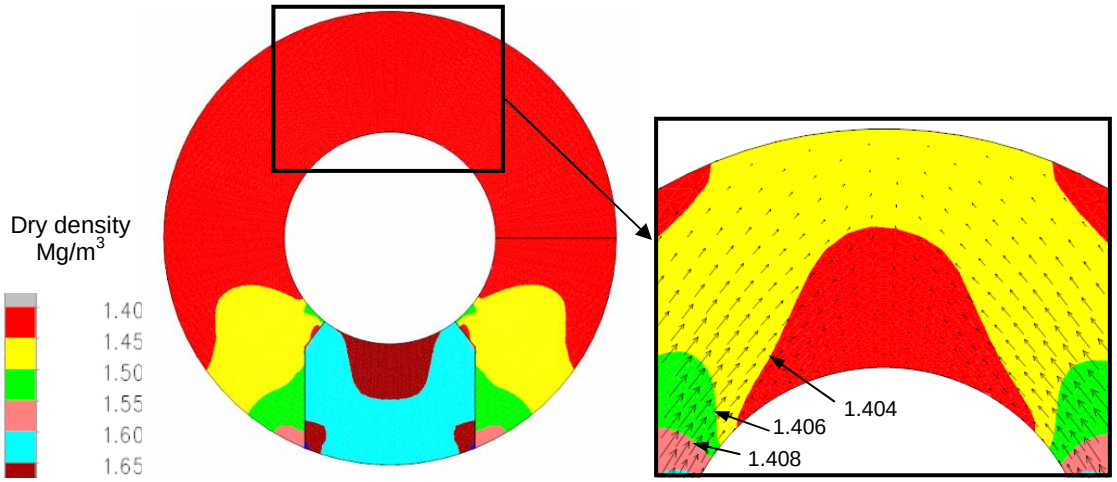


**Figure 9: Contour Plot of Dry Density with Detail of Region above the Container for the Case of Fresh Water and Initial Pellet Dry Density of 1.40 Mg/m$^3$.**

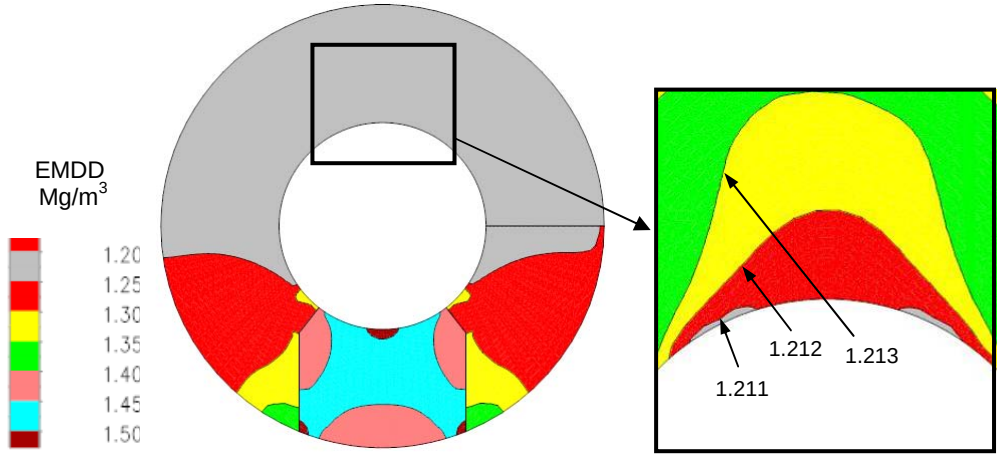


**Figure 10: Contour Plot of EMDD with Detail of Region above the Container for the Case of Fresh Water and Initial Pellet Dry Density of 1.40 Mg/m$^3$ or EMDD of 1.210 Mg/m$^3$.**

The equilibrium swelling pressure (mean stress) and density of the material in contact with the container were of greatest interest for assessing the protection of the container from microbial-influenced corrosion. Figures 11, 12 and 13 include plots of mean stress, dry density and EMDD, respectively, in the bentonite adjacent to the container at the different pore water salinities applied in the analyses. The results shown are for the case of 1.40 Mg/m$^3$ initial pellet dry density. Similar plots for initial pellet densities of 1.35, 1.45 and 1.50 Mg/m$^3$ are provided in Appendix B. As shown in Figures 12 and 13, the equilibrium dry densities and EMDD of the HCB pedestal were only slightly higher with increased pore water salinity. The higher pore water salinity reduced both the mean stress (Figure 11) and the amount of swelling expansion of the HCB pedestal resulting in higher density. Any effect of increasing salinity on pellet density was not apparent from the modelling results. Figures 12 and 13, however, show the density of bentonite pellets close to the pedestal was generally higher than the as-placed density at all salinities. The low spike in dry density for 350 g/L salinity was an artefact of the grid used in the analysis (Figure 7).

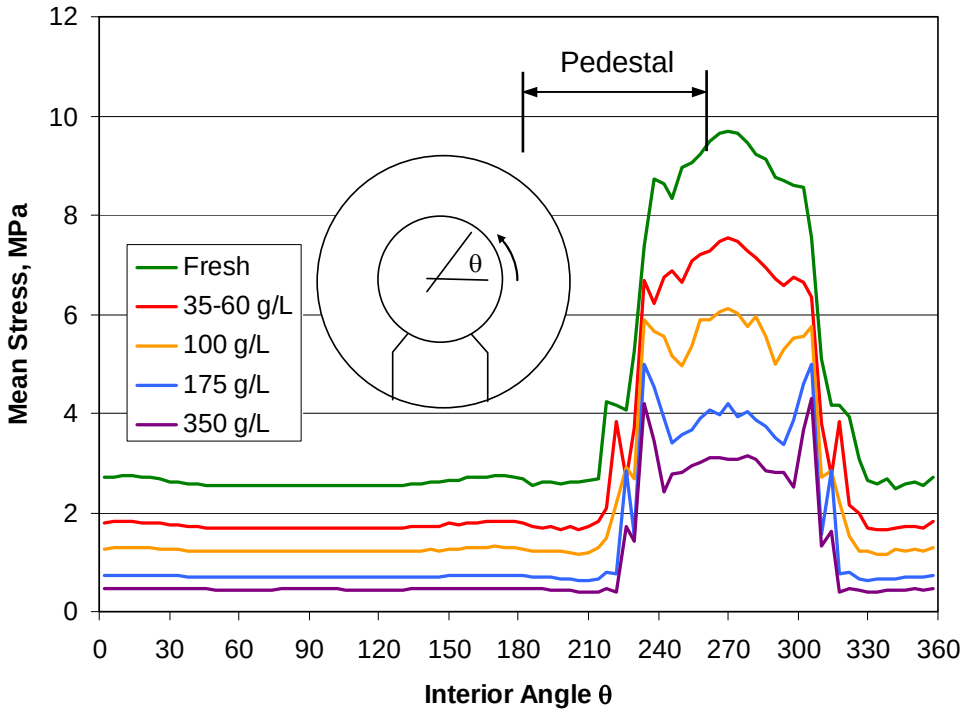


**Figure 11: Mean Stress in the Bentonite Adjacent to the Container Surface for the Case of Initial Pellet Density of 1.4 Mg/m$^3$.**

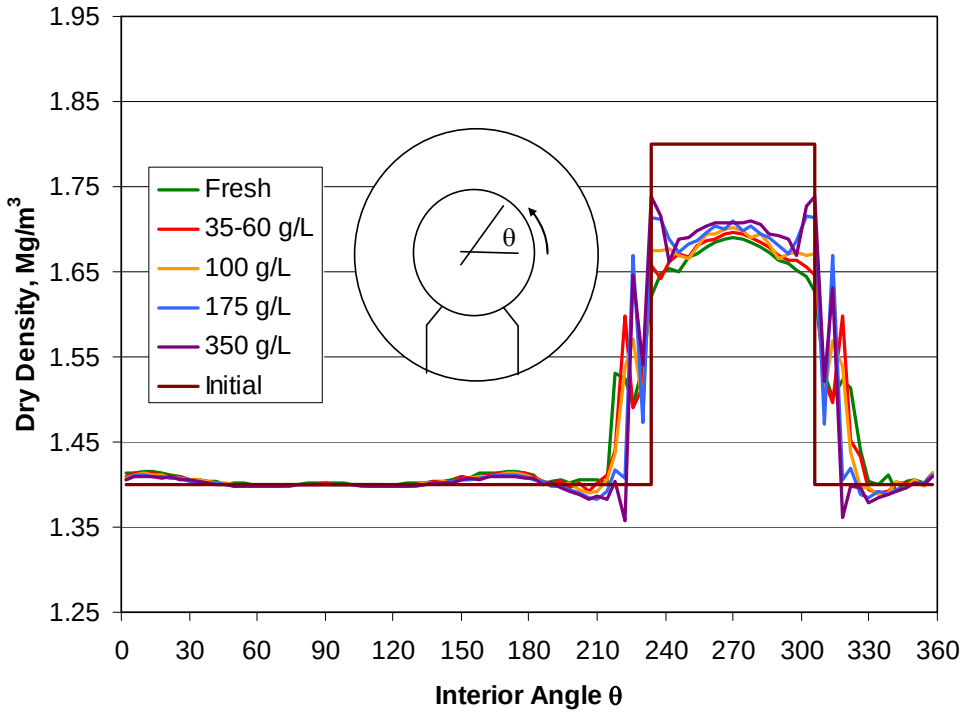


**Figure 12: Dry Density of the Bentonite Adjacent to the Container Surface for the Case of Initial Pellet Density of 1.4 Mg/m$^3$.**

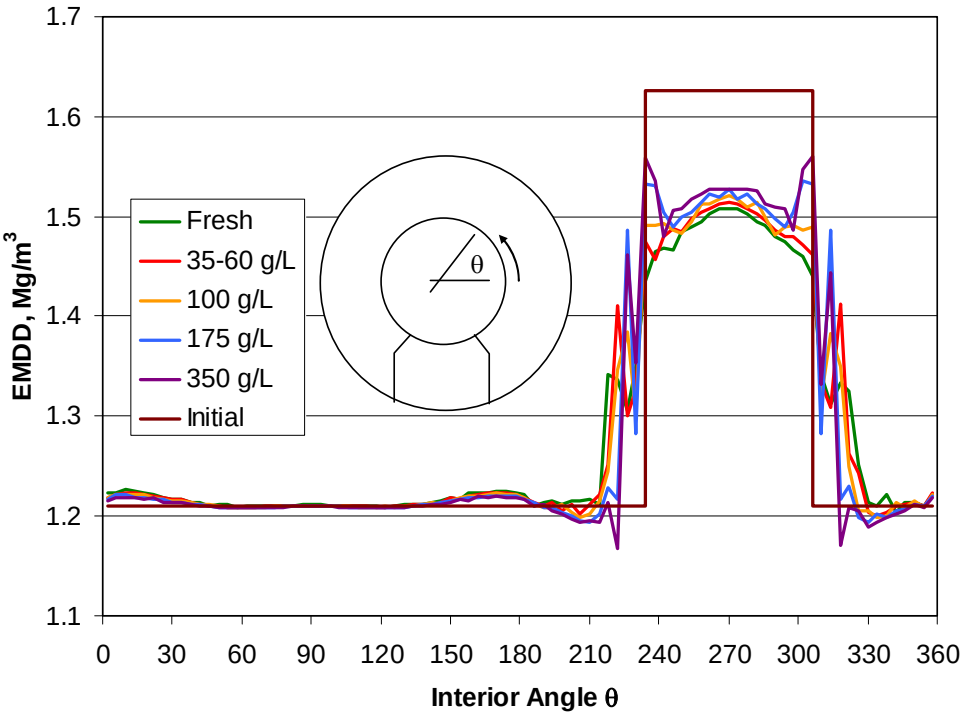


**Figure 13: EMDD of the Bentonite Adjacent to the Container Surface for the Case of Initial Pellet Density of 1.4 Mg/m$^3$.**

### 4.3 The Container Mass and Container Movement

Conceivably, the mass of the container can inhibit its upward movement caused by swelling of the HCB below it. Given that upward movement was small to start with, this observation seems moot. Still, two analyses were run with gravity turned on and the container mass set to approximately 6000 kg/m, one with fresh water and a second with a salinity of 350 g/L. The mass of the clay material was also allowed to contribute to decreased upward movement. The vertical movement of the container with and without gravity was 2.9 mm and 3.2 mm[4], respectively for the case of fresh water and an initial density of 1.40 Mg/m$^3$ initial pellet density. When the salinity was increased to 350 g/L, the vertical container movement was reduced to 1.5 mm from 1.6 mm without gravity. Consideration of the mass of the container had essentially no impact on the results of the analysis.

### 4.4 Loading-Unloading Hysteresis

Only the HCB pedestal expanded (unloaded) during the horizontal placement analysis. To consider the implications of loading-unloading hysteresis, the mean stress versus EMDD relationship for unloading, [9], was assigned to the HCB pedestal, while the bentonite pellets, which were under compression, maintained the original relationship, [3a]. Only the fresh water case was analysed, and the results are presented in Figure 14.

[4] This upward displacement does not take into consideration any initial downward movement caused by compression of the HCB pedestal upon initial placement of the container.

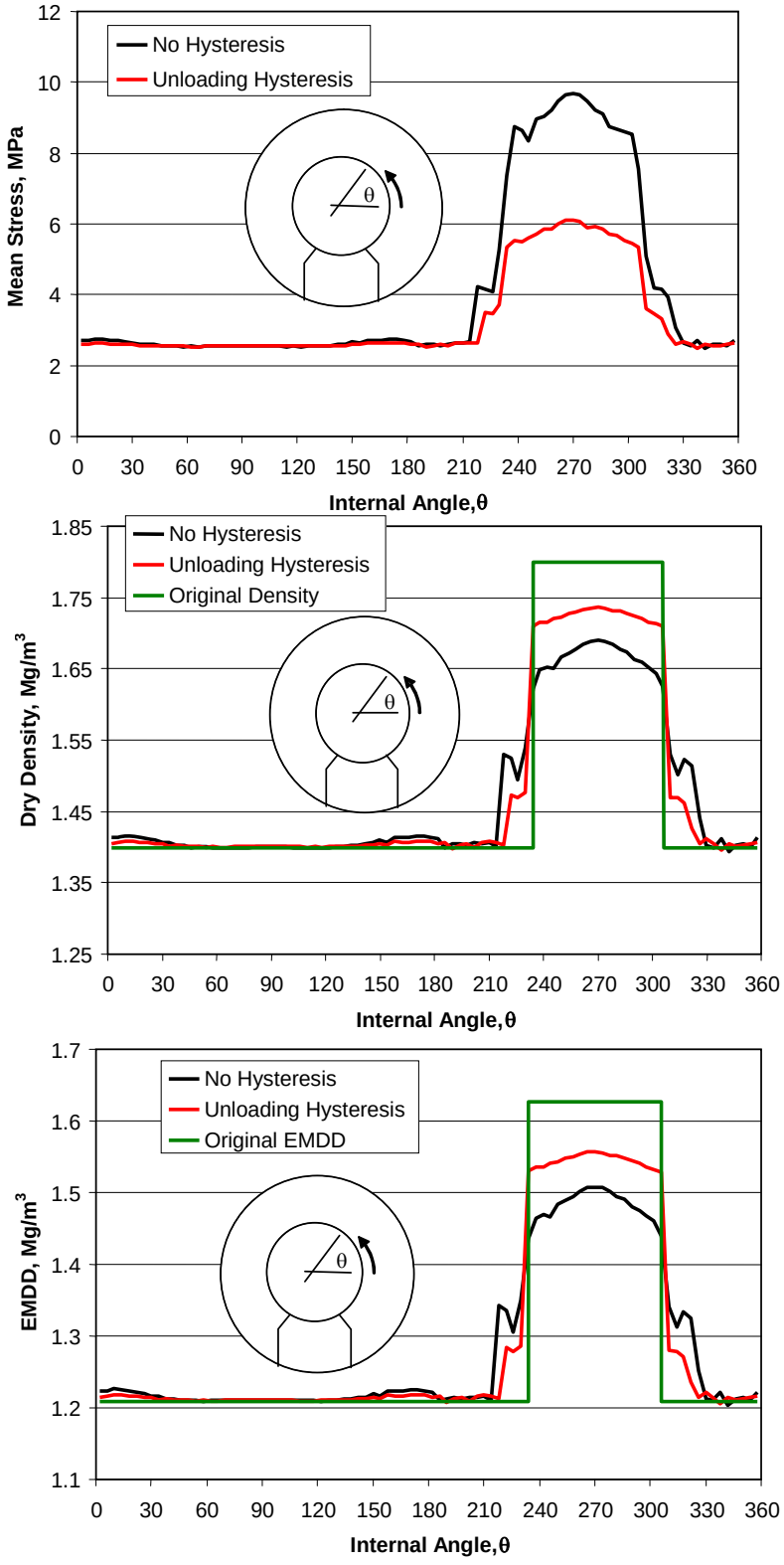


**Figure 14: Mean Stress, Dry Density and EMDD for Cases With and Without Unloading Hysteresis for a Simulation having 1.4 Mg/m$^3$ Initial Dry Density Pellets and Fresh Water.**

Compared with the no load-unload hysteresis analysis, the hysteresis model resulted in appreciable differences in stress and density for only the HCB pedestal. Upon unloading, the mean stress in the HCB pedestal was less for the case with no hysteresis. The dry density was also less for the case of no hysteresis indicating that volumetric expansion of the HCB was greater. Figure 14 shows that, for the horizontal placement design option, the HCB mean stress decreased by almost 40% when hysteresis was modelled, compared with the case in which loading and unloading followed the same stress path. However, the bentonite pellet mean stress was not greatly affected. The bentonite pellet density remained close to as-placed dry density for both the hysteresis and no hysteresis models.

### 4.5 Summary of Observations

Observations from inspection of the results of compliance analysis of the horizontal placement option include:

1. The expansion of the HCB pedestal had only a very local affect on the density of the bentonite pellets.
2. Since upward movement of the container was very small (a few mm) there is no apparent compression of the material above the container.
3. Salinity had little effect on density, particularly in the region of bentonite pellets.
4. Although the dry density of the bentonite pellets remained close to the as-placed density at all salinities, the mean stress (swelling pressure) decreased with increasing salinity. At 350 g/L of NaCL the mean stress in the bentonite pellets was less than 1 MPa for all initial pellet densities.

Saturation and swelling of the bentonite pellet material resulted in almost no change in dry density, and hence no change in EMDD for most of the bentonite pellet material regardless of salinity. Since there was no density change, the final mean stress (swelling pressure) in the bentonite pellet material could have been calculated beforehand using the appropriate form of equation [3a-e] and the bentonite pellet as-placed EMDD.

Bentonite pellets placed at a dry density of 1.4 $Mg/m^3$ remained at 1.4 $Mg/m^3$ upon achieving saturated equilibrium in the region above the container. This suggested that if the bentonite pellets can be placed at an initial dry density that is sufficient to inhibit microbial activity, the material will maintain this density regardless of the salinity of the pore fluid.

## 5. THE IN-FLOOR BOREHOLE PLACEMENT MODEL

### 5.1 Model Geometry

The in-floor borehole placement method involves the vertical placement of cylindrical containers in large diameter boreholes. The containers are surrounded by pre-compacted swelling clay blocks that fill most of the space between the container and the surrounding rock. Different design alternatives have been advanced in different countries over the years. The geometry used in the compliance modelling for this report was based on the room geometry provided by RWE NUKEM (2003). The cross-section of the borehole and emplacement room geometry is illustrated in Figure 15.

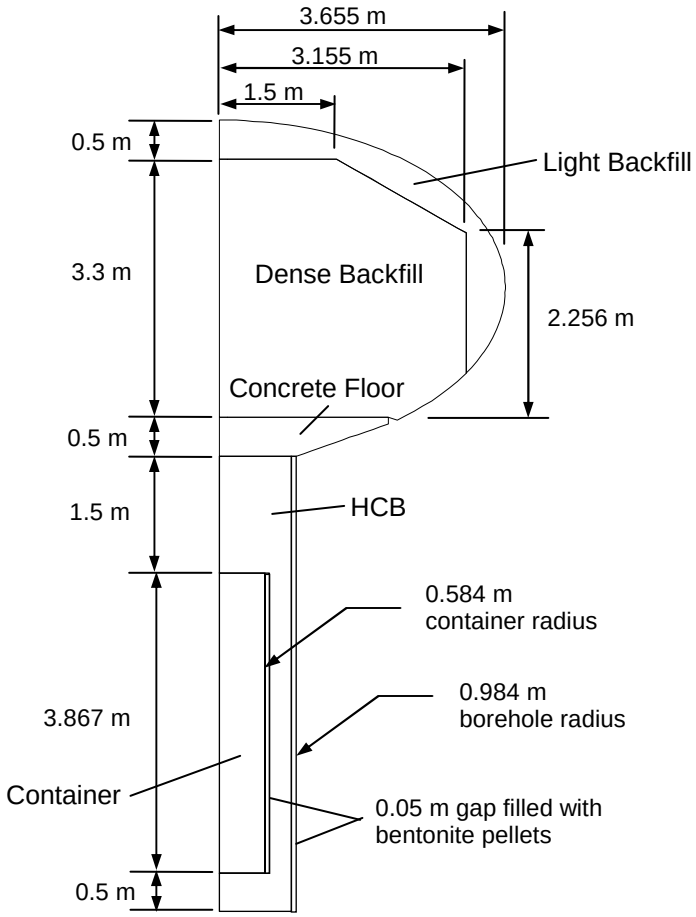


**Figure 15: Configuration of the Borehole Emplacement Model Considered in Compliance Modelling.**

The compliance model described in this report was a two-dimensional analysis. Using a two-dimensional axisymmetric geometry it was not possible to capture both the axisymmetry of the materials in the borehole and the tunnel above the borehole. To carry out the analyses using axisymmetry, the compliance modelling of the in-floor borehole placement method used two different model geometries:

1. The first model included only the material at the mid-height of the container (Figure 16). The model had a one-dimensional radial geometry for the material between the container and the rock.
2. The second model used two-dimensional axisymmetry to represent both the borehole and tunnel using a simplified tunnel geometry (Figure 17). Model geometries similar to the cross-sections shown in both Figures 15 and 17 were prepared and run, however, only the simplified longitudinal geometry in Figure 17 was considered to be representative of the average shape of the tunnel above the borehole. The radius of the tunnel room (3.0 m) was selected such that the volume of DBF and LBF above a single placement borehole would be similar to the material volumes between adjacent boreholes. The numerical model included the material in the tunnel above the borehole to evaluate the potential for swelling clay to push out of the borehole and into the room above.

## 5.2 Boundary Conditions

The initial stress in all three principal directions for the swelling clay was established by setting the stress in all three directions to be equal to the swelling pressure as defined by [3a] to [3e]. The initial stresses in the non-swelling materials (concrete, dense backfill and container) were set to zero.

The inside and outer edges of the one-dimensional model were prevented from moving radially, while the top and bottom of the model were prevented from moving vertically. For the two-dimensional model that included the tunnel above the placement borehole, vertical movement of the HCB out of the borehole was allowed by placing DBF directly above the borehole instead of concrete. Simulations were run using both friction between the upward moving HCB and the rock and with frictionless HCB-rock interfaces. Frictionless surfaces represented the upper limiting case for HCB expansion, thus allowing the greatest density reduction from as-placed conditions.

The container was a simulated as a rigid block and hence was allowed to be pushed up or down as the HCB expanded upon saturation.

## 5.3 As-placed Properties

There were four different clay materials in the model; these materials included HCB, bentonite pellets (gap fill), dense backfill (DBF), and light backfill (LBF). The initial density and composition of LBF and DBF are provided in Table 1. Since LBF was modelled as a swelling clay, its initial stress was determined using [3a] and its Bulk and Shear Moduli were determined using [5] and [6], respectively. DBF was modelled as an elastic solid with a constant Bulk Modulus of 26 MPa and Poisson's Ratio of 0.3, as discussed in Section 3.4.

A sensitivity analysis was performed by varying the following quantities:

- the initial density of the bentonite pellets,
- the width of the pellet-filled gaps between the HCB and the rock and between the HCB and the container, and
- the initial density of the HCB.

The different parameters used in the sensitivity analysis are summarized in Table 2. The reference initial densities and gap thicknesses were taken from Hobbs et al. (2005), although more recent studies have demonstrated that higher as-placed densities than those listed by Hobbs et al. (2005) are possible. Including the reference case, twenty-one different sets of density and gap thickness parameters were used in the analyses. The sensitivity analysis was first performed with no hysteresis and then repeated with hysteresis (different loading and unloading paths). Selected combinations of initial conditions were then reanalysed using four different pore water salinities (for the model without hysteresis only) for a total of 57 simulations.

The potential for hysteresis between loading and unloading paths for HCB was discussed in Section 3.5. In the borehole placement option, expansion of the HCB resulted in the compression of the bentonite gap fill between the HCB and the container. If expansion of HCB follows the unloading path in Figure 5, then less expansion will occur. Correspondingly, less compression of the gap fill, and a lower gap fill density, compared to the no hysteresis case, was expected. The sensitivity analysis in Table 2 was repeated using [9] for the HCB to represent load-unload hysteresis. As noted in Section 3.5, experimental data are currently

insufficient to produce a model for unloading under saline conditions. Therefore, all analyses involving hysteresis were performed using only a fresh water permeant.

**Table 2: Parameters used in Borehole Emplacement Model Sensitivity Analysis**

| | HCB as-placed dry density ($Mg/m^3$) | Gap width (mm) | Bentonite gap fill as-placed dry density ($Mg/m^3$) |
|---|---|---|---|
| Reference[5] | 1.61 | 50 | 1.4 |
| Sensitivity Analyses | 1.7 | 30 | 1.3, 1.35, 1.4, 1.45 and 1.5 |
| | | 50 | 1.3, 1.35, 1.4, 1.45 and 1.5 |
| | 1.8 | 30 | 1.3, 1.35, 1.4, 1.45 and 1.5 |
| | | 50 | 1.3, 1.35, 1.4, 1.45 and 1.5 |

## 5.4 Results

Results from the simulation using the reference densities and dimensions were used to assess the impact of the following two specific modelling assumptions.

1. The assumption that the results from the two-dimensional model that included both the borehole and tunnel were similar to the results from the one-dimensional model at the container mid-height.
2. The assumption that the results from the two-dimensional model with a frictionless borehole surface were similar to the results from a model that included friction between the clay and the rock. For the simulation that used sidewall friction, the angle of internal friction between the clay and the rock was arbitrarily set to 25º.

Sensitivity analyses were used to compare the final densities of the HCB blocks and the bentonite pellet gap fill material as a function of the initial pellet density, the initial HCB block density and the gap thickness. The results could be used to identify those combinations of initial densities and gap thickness that would produce an optimum minimum target dry density adjacent to the container, such as the 1.4 $Mg/m^3$ suggested by Stroes-Gascoyne and Hamon (2008).

### 5.4.1 Final Densities and Mean Stress in the One- and Two-Dimensional Models

The final densities at the container mid-height for three different simulations are compared in Figure 18, while the final stresses within the bentonite are compared in Figure 19. The three simulations were the reference case with a one-dimensional geometry, with a two-dimensional axisymmetric geometry and no wall friction, and the axisymmetric geometry with friction at the bentonite-rock interface. At the container mid-height, all three simulations produced identical results for dry density and stress (Figures 18 and 19). Expansion of the HCB upon saturation was accompanied by a compression of the bentonite gap fill for all cases. The end result was a 3 % reduction in HCB density and a corresponding increase in gap fill density by 9%. The gap

[5] Material densities and gap thickness provided in Hobbs et al. 2005

fill remained in close contact with the container surface and imparted a radial contact pressure of 4.4 MPa.

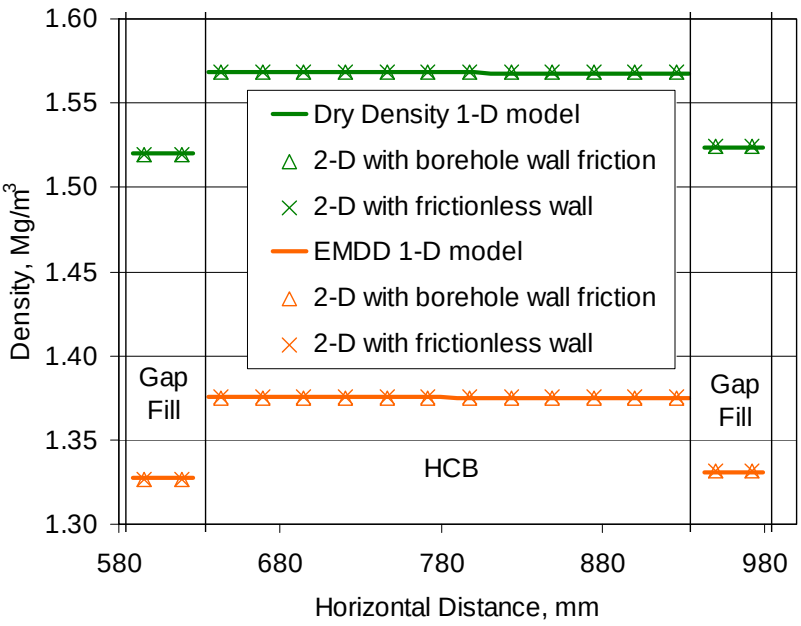


**Figure 18: Dry density and EMDD versus Horizontal Distance from the Centre of the Borehole for the Reference Initial Densities and Three Different Modelling Cases.**

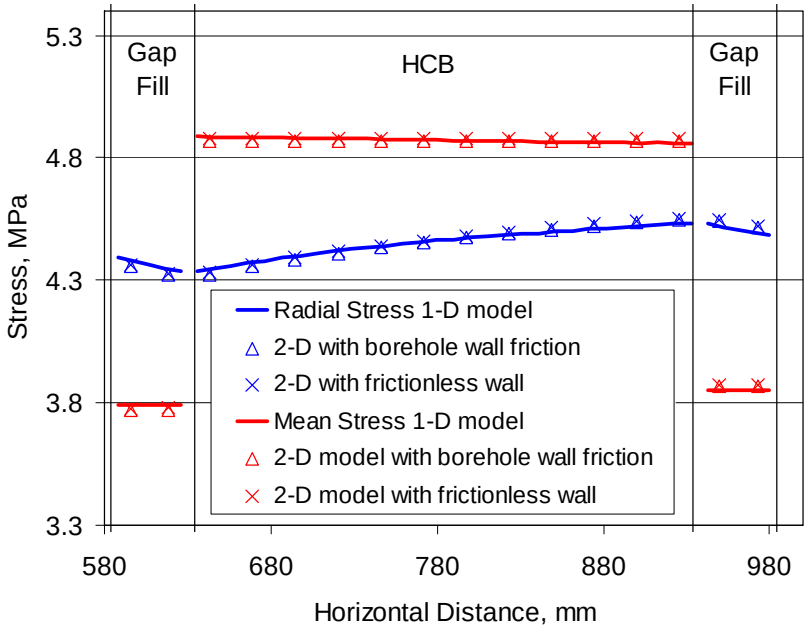


**Figure 19: Mean Stress and Radial Stress versus Horizontal Distance from the Centre of the Borehole for the Reference Initial Densities and Three Different Modelling Cases.**

### 5.4.2 Vertical Container Displacement With and Without Wall Friction

The vertical displacement of the container and HCB along the central axis of the borehole for the reference case is illustrated in Figure 20. The upward movement of the container was about 7.6 mm for the simulation with no sidewall friction, and 2.4 mm for the simulation with sidewall friction. The displacement of the top of the HCB due to compression of the tunnel backfill materials was approximately 40 mm for both the simulations with and without sidewall friction. Although there was no difference in the computed HCB and gap fill densities (Figure 18), the simulation that incorporated a frictionless wall predicted greater upward movement of the container.

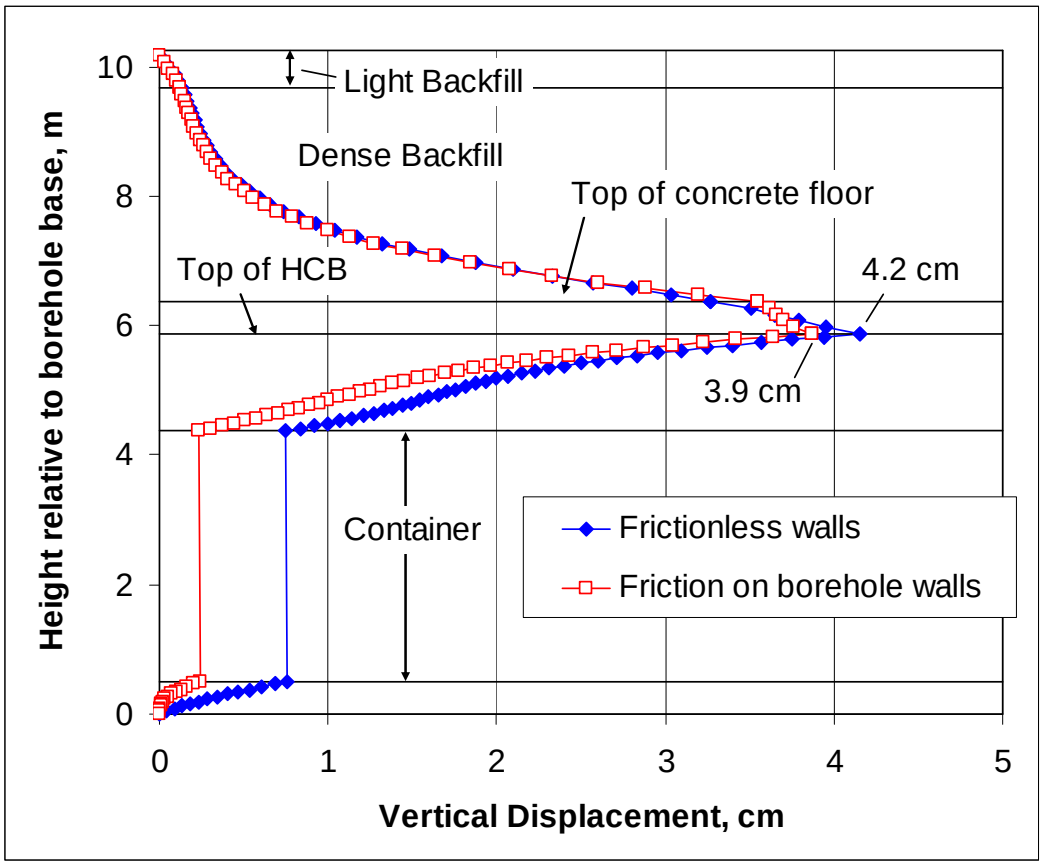


**Figure 20: Vertical Displacement of Clay Materials and the Container along the Central Axis of the Models with and without Sidewall Friction.**

### 5.4.3 Variation of Dry Density around the Container

The HCB density above and below the container was greater than in the annulus between the container and the rock. The dry density of the HCB above and below the container was only slightly decreased from the as-placed densities (Figure 21). In these regions, the HCB was more distant from the gap fill and the material was better constrained against volumetric expansion. The displacement vectors shown in Figure 21 indicate a general upward movement of all materials within the emplacement borehole. The directions of the vectors also illustrate

the expansion of the HCB and concurrent compression of the gap fill in the annular region of the borehole.

The bentonite pellets filling the gap between the HCB and the container had a lower density than the HCB that surrounded it. Except for the top and bottom few centimetres of gap fill, the density of the pellet material in contact with the container was nearly constant along its length. This indicated that the one-dimensional model at the container mid-height provided results that were representative of the entire gap fill material surrounding the container. The density within a few centimetres of the top and bottom of the gap (Figure 21) was slightly less than the density of most of the gap fill (1.48 Mg/m$^3$ compared to 1.52 Mg/m$^3$ for the reference case). This localised density reduction was related to the HCB and gap fill being represented in the model as a bonded continuum. Differential displacement within the HCB near the 90º corner of the container resulted in a reduction in density of the more compliant material at that location, which was the gap fill. It is probable that the computed density reduction of this small volume of gap fill was related to an HCB-gap fill interface that did not reflect actual interface behaviour.

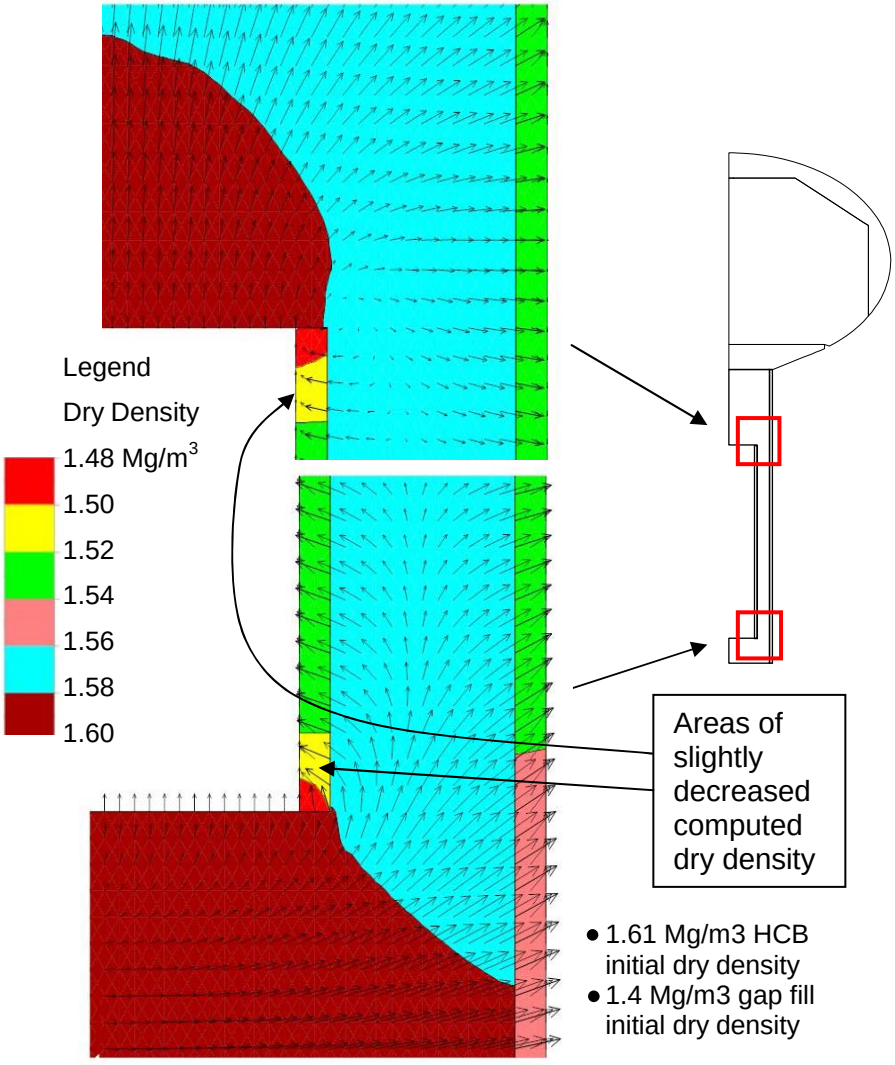


**Figure 21: Dry Density Contours and Clay Displacement Vectors near the Top and Bottom of the Container for the Reference Density Model.**

### 5.4.4 Sensitivity Analysis of Gap Fill Dry Density Adjacent to the Container

Higher bentonite density leads to a decrease in the potential for microbial-influenced container corrosion. Therefore, the final density of the gap fill material adjacent to the container was the output parameter of greatest interest. Initial placement densities for the bentonite pellets in the gaps between the HCB and the container and between the HCB and the rock were varied from 1.3 Mg/m$^3$ to 1.5 Mg/m$^3$. The final HCB and gap fill dry densities as a function of placement density and gap thickness is provided in Figures 22 and 23 for initial HCB dry densities of 1.7 Mg/m$^3$ and 1.8 Mg/m$^3$, respectively. The material response was assumed to follow the same loading and unloading path for the results presented in both Figure 22 and Figure 23. The results were taken from the one-dimensional model, which was shown in the previous sections to be representative of gap fill and HCB densities throughout the annular region around the container.

For all cases analysed, the a final gap fill dry density of 1.4 Mg/m$^3$ was exceeded if the as-placed gap fill dry density was at least 1.3 Mg/m$^3$. The lowest final gap fill dry density was 1.54 Mg/m$^3$ for the case having an initial HCB dry density of 1.7 Mg/m$^3$ and a gap width of 5 cm. In practice, Martino and Dixon (2006) were able to achieve a bentonite pellet dry density of 1.41 Mg/m$^3$ (and EMDD of 1.22 Mg/m$^3$) in a 5 cm gap simply by pouring.

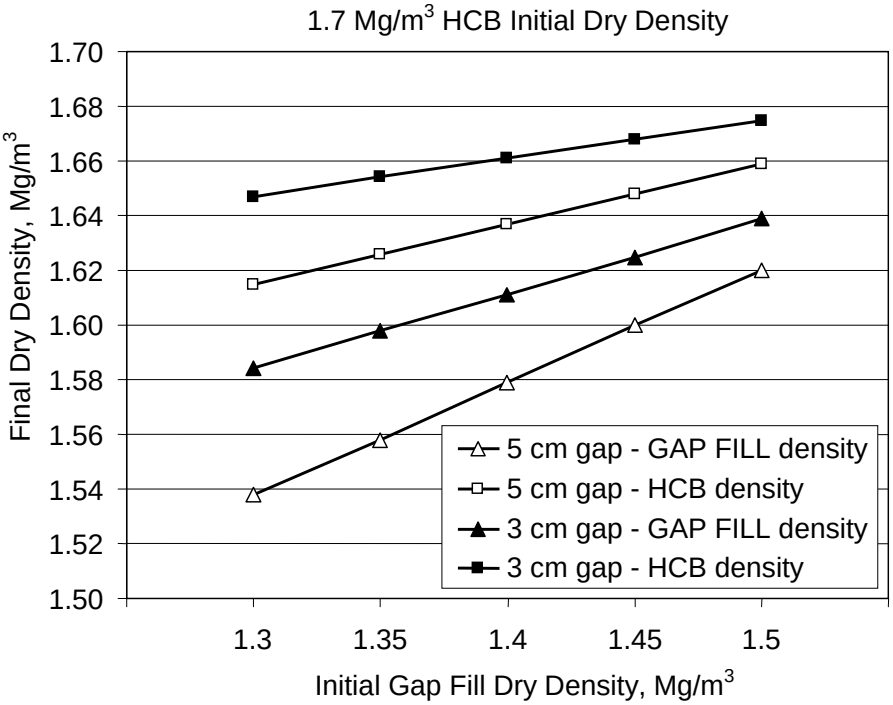


**Figure 22: HCB and Gap Fill Dry Density as a Function of Placement Density and Gap Thickness for Initial HCB Density of 1.7 Mg/m$^3$.**

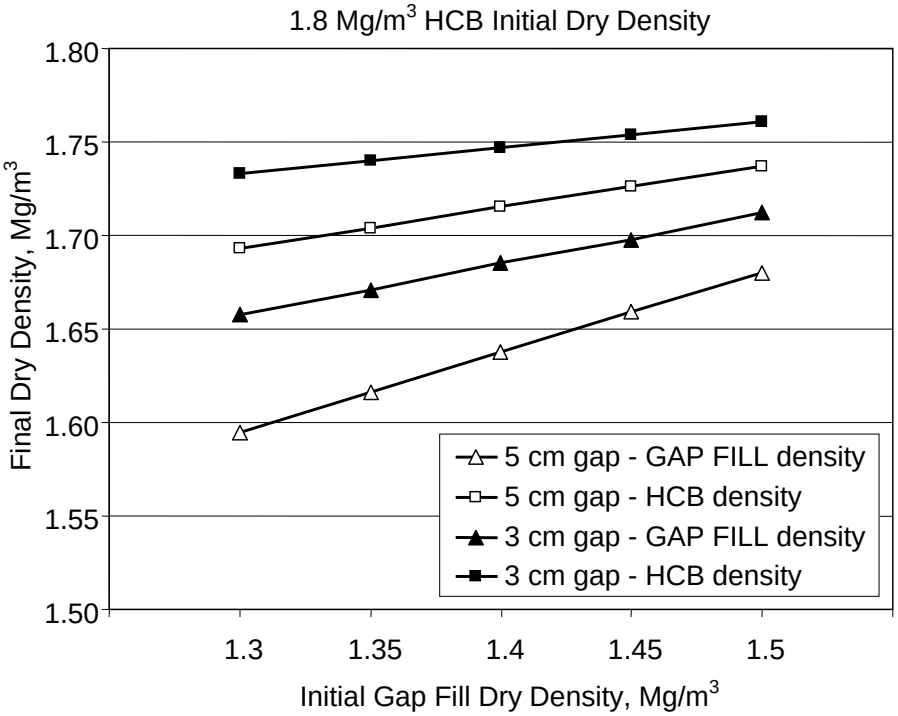


**Figure 23: HCB and Gap Fill Dry Density as a Function of Placement Density and Gap Thickness for Initial HCB Density of 1.8 Mg/m$^3$.**

### 5.4.5 Effect of Salinity

The results presented in Section 5.4.4 were for fresh water conditions only. The influence of saline pore water on the final density of the gap fill material adjacent to the used-fuel container was implemented by using Equations [3b] to [3e] to define the relationship between mean stress (swelling pressure) and EMDD. The analysis was repeated for initial gap fill dry densities from 1.3 to 1.5 Mg/m$^3$ and for initial HCB dry densities of 1.7 and 1.8 Mg/m$^3$. Only a gap thickness of 5 cm was used in the analyses. The final density of the gap fill material is illustrated in Figure 24.

Although the analyses were conducted at four different salinity conditions (35 to 60 g/L, 100 g/L, 175 g/L and 350 g/L) only the 350 g/L results are illustrated in Figure 24. There was very little difference between the results from the fresh water case and that of the highest saline pore fluid analysed. The decrease in the gap fill dry density due to an increase in salinity from fresh water to 350 g/L was less than 0.01 Mg/m$^3$ for all cases analysed. Although the swelling pressure generated by the HCB was decreased by the presence of saline pore fluid, the high salinity also decreased the bulk modulus of the gap fill making it more compliant and more readily compressed to higher densities. These two influences had the effect of offsetting one-another and result was almost no effect of salinity on final density. Although the relative quantities of HCB and bentonite pellets (gap fill) are very different, the in-room placement and in-floor borehole placement options produce the same basic observation: that the final density of the gap fill or bentonite pellets was relatively unaffected by pore water salinity.

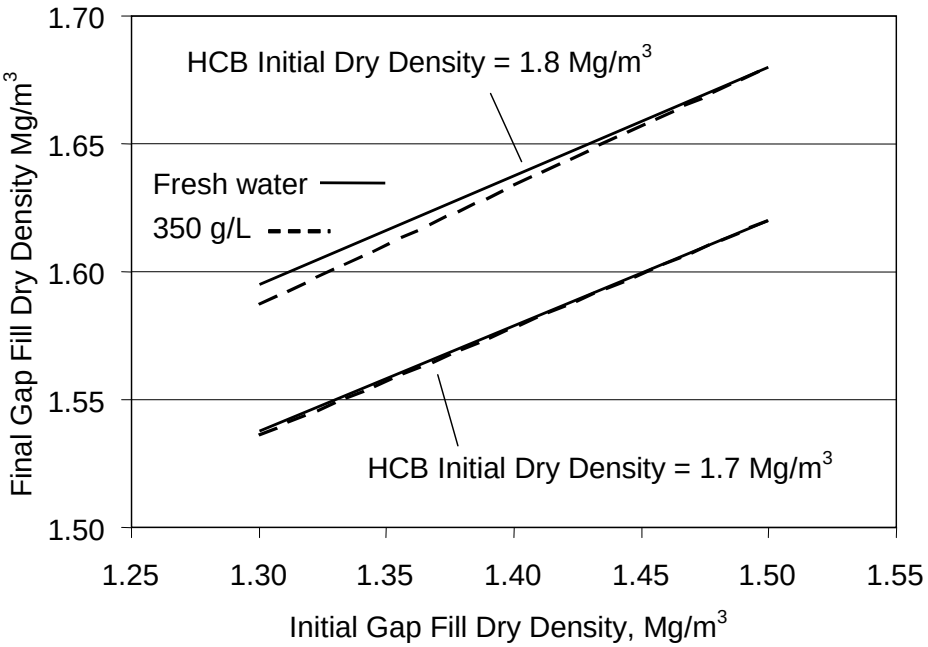


**Figure 24: Final Gap Fill Dry Density as a function of salinity and initial dry density for a 5 cm gap thickness.**

### 5.4.6 Effect of Loading-Unloading Hysteresis

The results presented in the preceding sections were for a material behaviour model without hysteresis. It was evident from laboratory tests performed on HCB that compacted bentonite did not expand along its loading path when the applied stress is removed (Figure 4). The relationship between EMDD and applied stress during unloading, as presented in Figure 5, is very preliminary and needs further experimental verification. However, it was worthwhile to assess the potential impact of hysteresis by using the relationship in [9] to define the unloading response of the HCB. Compression (loading) of the gap fill material was represented by using the EMDD versus mean stress relationship in [3a]. The final HCB and gap fill dry densities computed with hysteresis included are presented in Figures 25 and 26. As was the case with the in-room placement analysis, results from experiments using saline pore fluid were too preliminary to establish a definitive mean stress versus EMDD relationship during unloading. Therefore only fresh water analyses were run for analyses that included hysteresis.

The final gap fill densities, computed using the hysteresis model, were not as high as the density results for the model with no hysteresis. Volume expansion of the HCB during unloading was reduced when the hysteresis relationship, [9], was used. Reduced HCB expansion resulted in reduced compression of the gap fill. However, a final gap fill dry density of 1.4 Mg/m$^3$ was still exceeded if the as-placed gap fill dry density was at least 1.3 Mg/m$^3$. The lowest final gap fill dry density was 1.42 Mg/m$^3$ for the case having an initial HCB dry density of 1.7 Mg/m$^3$ and a gap width of 5 cm (as compared with 1.54 Mg/m$^3$ for the model without hysteresis using the same initial material properties).

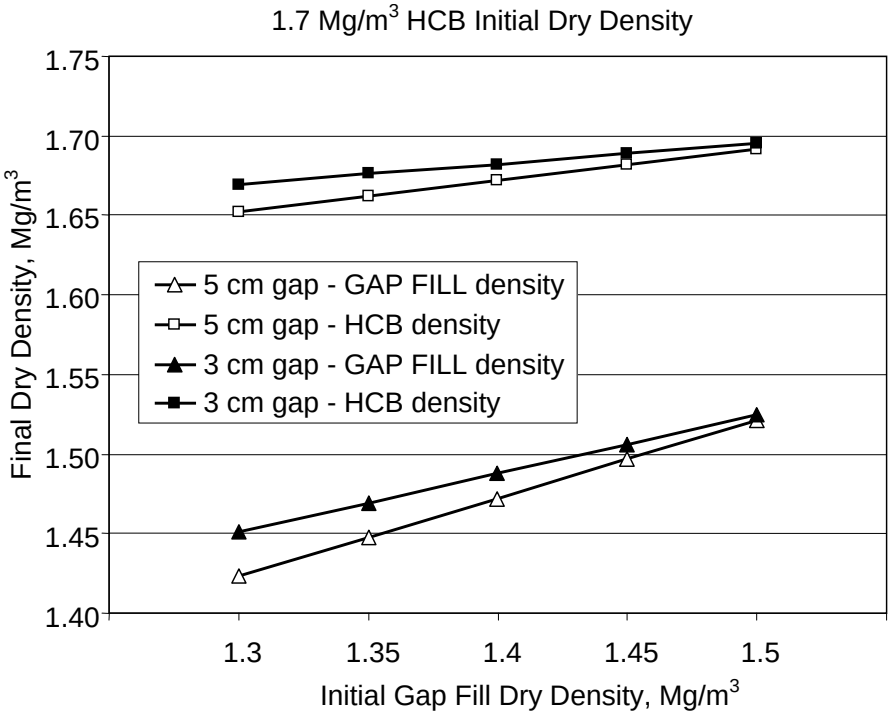


**Figure 25: Results from the Hysteresis Model Showing HCB and Gap Fill Dry Density as a Function of Placement Density and Gap Thickness for Initial HCB Density of 1.7 Mg/m$^3$.**

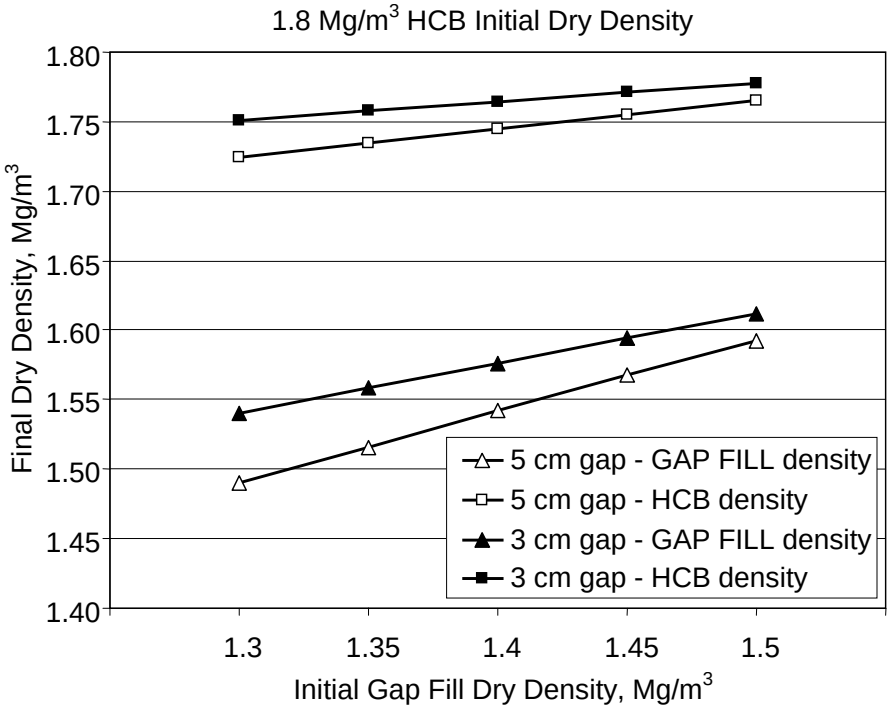


**Figure 26: Results from the Hysteresis Model Showing HCB and Gap Fill Dry Density as a Function of Placement Density and Gap Thickness for Initial HCB Density of 1.8 Mg/m$^3$.**

## 5.5 Summary of Observations

Observations from inspection of the results of compliance modeling of the borehole placement method include:

1. The final dry density of the HCB blocks and the bentonite pellets placed in the gaps was very uniform throughout the annulus between the container and the rock. Because of this uniformity, the one-dimensional model at the container mid-height produced similar results to the two-dimensional axisymmetric model.
2. The final dry density of both the HCB and gap fill was increased by using a higher initial as-placed density of either the HCB or the gap fill material. However, the final density of the HCB blocks was always higher than the final density of the gap fill (i.e., density homogenisation did not occur).
3. The final dry density of both the HCB and gap fill was increased by decreasing the gap width from 5 cm to 3 cm. The increase in gap fill dry density was about 0.05 $Mg/m^3$ for most analyses that used 1.3 $Mg/m^3$ as the initial gap fill dry density.
4. Saline pore fluid up to 350 g/L had almost no effect on the final density of the gap fill adjacent to the used-fuel container. However, this observation applies only to the analysis without hysteresis.
5. There was a slight reduction in computed density (about 0.04 $Mg/m^3$) in the gap fill adjacent to the container at the very top and bottom of the container. This computed reduction was probably related to the numerical treatment of the interface of the HCB and gap fill as a bonded continuum.
6. Vertical displacement of the container and of the HCB at the top of the placement borehole was obtained from the simulation results. However, the magnitude of displacement was variable and was dependent upon the material properties as well as the representation of the interfaces between the materials and at the rock surface. Whether or not these interfaces were assigned friction coefficients, or were treated as being fully bonded affected the ultimate magnitude of the computed vertical displacement.
7. The results from the numerical analyses suggested that the final dry density of the bentonite gap fill adjacent to the used-fuel container would be greater than 1.4 $Mg/m^3$ if all the following initial conditions were satisfied:
    i. an initial gap fill dry density of at least 1.3 Mg/m3;
    ii. an initial HCB dry density of at least 1.7 Mg/m3; and
    iii. gap widths between the container and bentonite blocks and between the bentonite blocks and the rock of 5 cm or less.
8. Although the selection of either a hysteresis or no hysteresis material behaviour model had the greatest influence on the resulting computed material dry densities, the gap fill dry density adjacent to the used-fuel container was still greater than 1.4 $Mg/m^3$ for the initial conditions listed in observation 6 (above).
9. The final gap fill dry density computed by the model that included hysteresis was much lower than the results from the model without hysteresis. For example, the final gap fill dry density with hysteresis was 1.42 $Mg/m^3$ and without hysteresis was 1.54 $Mg/m^3$, for initial gap fill and HCB dry densities of 1.3 and 1.7 $Mg/m^3$, respectively, and an initial gap width of 5 cm. Although the model with hysteresis is a better representation of material behaviour, there is less data available to define the model parameters. Further refinement of the hysteresis model is recommended before definitive conclusions are made with respect to the density computed using compliance modelling.

## 6. DISCUSSION

Compliance modelling can provide insight into the density changes of the swelling clay upon saturation. The modelling is useful if a design objective is to achieve a specific minimum dry density at the surface of used-fuel containers in order to minimise the potential for microbially-influenced corrosion of the container. The input requirements for compliance modelling include the design geometry, the as-placed material densities and a relationship between density and mean stress for each material. The materials can also be allowed to have different relationships depending upon pore water salinity and whether the material is expanding or compressing.

There is an increasing database of information that relates the montmorillonite content of the bentonite and the bentonite's dry density with its swelling pressure. Swelling pressure is typically determined using tests in which the stress is known only in one direction. For the purpose of developing material properties for the compliance model, the axial stress from these tests has been assumed to be equivalent to the swelling pressure or mean stress. This will not be the case if the lateral stress in the test cell, which is not measured, is not equal to the applied axial load. The compliance modelling described in this report uses a Poisson's Ratio of 0.4 for all swelling materials. This value has very little evidential support and was used in the absence of more conclusive experimental data. However, mean stress is only equal to the axial stress if Poisson's Ratio equals 0.5 and the material behaves like a fluid. Using a lower Poisson's ratio introduces a contradiction between the assumptions that the material does not behave like a fluid and that axial stress equals mean stress. It would be prudent to examine the shear behaviour of swelling clay before assigning too much importance to the use of compliance modelling as a tool for comparing different design options.

## 7. CONCLUSIONS

Compliance modelling was used to compute the potential change in density of two different canister placement alternatives: a horizontal borehole option, and a vertical in-floor borehole option. The objective of the numerical modelling was to compute the long-term dry density of the bentonite material adjacent to the used-fuel container after saturation. A higher density bentonite will have the beneficial effect of minimising microbial activity and thus minimising microbially-influenced corrosion of the container. Research by others (Stroes-Gascoyne and Hamon, 2008) indicates that bentonite dry densities above 1.4 $Mg/m^3$ will result in microbe culturability being at or below background levels.

### Horizontal Borehole Placement

The analysis of the horizontal placement option was carried out using an HCB pedestal dry density of 1.80 $Mg/m^3$ and varying pellet material as-placed dry densities (1.35 to 1.50 $Mg/m^3$) and pore water salinities (0 to 350 g/L TDS). The fresh water case was repeated using a different mean stress versus density relationship for the expanding HCB than for the compressing bentonite pellets in an effort to simulate observed hysteresis based on loading and unloading portions of consolidation tests on bentonite.

The main observation from the compliance modelling was that the density of almost all the bentonite pellet material adjacent to the container was unchanged from its as-placed density

regardless of pore water salinity. The observation was the same for the cases with and without hysteresis. The implication is that for a minimum dry density of 1.4 Mg/m$^3$ to be achieved the bentonite pellets will need to be placed at 1.4 Mg/m$^3$. The compliance modelling also suggests that if the material is placed at 1.4 Mg/m$^3$ it will not decrease from that value after saturation, even if the pore water salinity is high. The final dry density of the bentonite pedestal was affected by the as-placed density of the bentonite pellets, by the pore water salinity and by whether or not the model considered the hysteresis effect. However, in all cases, the final HCB density was higher than the final density of the bentonite pellets, and was much higher than 1.4 Mg/m$^3$ (in fact, the HCB dry density was higher than 1.6 Mg/m$^3$ for all simulations).

**In-floor Borehole Placement**

The in-floor borehole placement option was simulated using a two-dimensional axisymmetric geometry that included the material in the tunnel above the borehole. Results showed that the gap fill material (bentonite pellets) and the HCB in the annular region surrounding the container was nearly constant for the entire length of the container. The computed density in both materials was almost identical to the density computed using a one-dimensional model that represented the mid-height of the container within the vertical borehole. The one-dimensional model was then used to conduct a sensitivity analysis using two as-placed HCB dry densities (1.7 and 1.8 Mg/m$^3$), a range of gap fill as-placed dry densities (1.30 to 1.50 Mg/m$^3$) and two different gap widths (3 cm and 5 cm). The analysis was repeated using different mean stress versus density relationships for the expanding HCB and the compressing bentonite pellets in order to simulate hysteresis.

The final dry density of the bentonite gap fill material adjacent to the container was dependent on all the input parameters that were varied as part of the fresh water sensitivity analysis. However, the computed final dry density of the gap fill was greater than 1.4 Mg/m$^3$ for all simulations. This observation is applicable to the analyses with as-placed HCB and gap fill densities as low as 1.7 and 1.3 Mg/m$^3$, respectively, and for analyses having gap widths as large as 5 cm. Although the gap fill density was less for the analyses that included hysteresis, the final dry density of the gap fill using the hysteresis model was still greater than 1.4 Mg/m$^3$. Other observations from the in-floor borehole placement compliance analyses are listed below.

1. The dry density of the gap fill upon complete saturation can be increased by:
   - Increasing the as-placed dry density of the gap fill material;
   - Increasing the as-placed HCB dry density from 1.7 to 1.8 Mg/m$^3$; and
   - Reducing the gap width from 5 cm to 3 cm.
2. In comparison with the model with no hysteresis, the model with hysteresis predicts lower final gap fill dry density upon complete saturation. For example, the lowest computed gap fill dry density was 1.42 Mg/m$^3$ for a simulation that included hysteresis and was 1.54 Mg/m$^3$ for the same simulation without hysteresis. Although the hysteresis model is a more appropriate description of the behaviour of the material, the parameters used as input into the model are based on relatively few tests. In addition, there is currently insufficient experimental data available to prepare a hysteresis model that can be used for saline pore water analyses (although testing is in progress).
3. Increasing the pore water salinity to 350 g/L had almost no effect on the final dry density of the gap fill material in contact with the used-fuel container for analyses without hysteresis. Although it seems intuitive the preceding observation would also apply to analyses with hysteresis, it cannot be stated definitively without first performing a saline pore water hysteresis simulation.

The results highlight the benefit in using higher density (1.8 Mg/m$^3$) HCB blocks and in reducing the width of the construction gaps that are to be filled with bentonite pellet material. The results also highlight the current deficiencies in the compliance modelling. The results of the model are greatly dependent upon whether or not loading-unloading hysteresis is considered when selecting the appropriate relationship between density and mean stress. The benefit of using compliance modelling for comparing different design options would be improved with enhanced understanding of the swelling clay behaviour under both saline and fresh water conditions.

## REFERENCES

Baumgartner, P. 2005. Scoping analyses for the design of a deep geologic repository in sedimentary rock. Ontario Power Generation Report 06819-REP-01300-10093-R00.

Baumgartner, P. 2006. Generic thermal-mechanical-hydraulic (THM) data for sealing materials – Volume 1: Soil - water relationships. Ontario Power Generation Nuclear Waste Management Division Report 06819-REP-01300-10122-R00.

Baumgartner, P., D. Priyanto, J.R. Baldwin, J.A. Blatz, B.H. Kjartanson and H. Batenipour. 2008. Preliminary results of one-dimensional consolidation on bentonite clay-based sealing components subjected to two pore-fluid chemistry conditions. Nuclear Waste Management Organization Report NWMO TR-2008-04.

Hobbs, M.Y., Gierszewski, P., A. D'Andrea, F. Garisto, M.R. Jensen, T.F. Kempe, P. Maak, S.B. Russell, G.R. Simmons, A. Vorauer, K. Wei. 2005. Deep Geologic Repository Technology Program – Annual report 2004. Ontario Power Generation, Nuclear Waste Management Division Report 06819-REP-01200-10146-R00.

Kjartanson, B. H., D.A. Dixon, and S. Stroes-Gascoyne. 2003. Effects of container/buffer gap fill on buffer performance. Ontario Power Generation, Nuclear Waste Management Division Report 06819-REP-01200-10102-R00.

Kjartanson, B.H., D.A. Dixon and C.L. Kohle. 2005. Placement of bentonite pellets to fill repository sealing system voids and gaps. Ontario Power Generation, Nuclear Waste Management Division Report 06819-REP-01200-10136-R00.

Maak, P. and S. Stroes-Gascoyne. 2008. Microbial impact on selecting the repository sealing system designs. In: Proc. International High-Level Radioactive Waste Management Conference, Sept. 2008, Las Vegas.

Martino, J.B. and D.A. Dixon. 2006. Placement and formulation studies on potential light backfill and gap fill materials for use in repository sealing. Ontario Power Generation, Nuclear Waste Management Division Report 06819-REP-01300-10011-R00.

NAGRA (Nationale Genossenshaft für die Lagerung Radioaktiver Abfälle). 2002. Project Opalinus Clay: Safety Report – Demonstration of disposal feasibility for spent fuel, vitrified

high-level waste and long-lived intermediate-level waste (Entsorgungsnachweis). NAGRA Technical Report 02-05.

Priyanto, D.G., J. A. Blatz, G. A. Siemens, R. Offman, J. S. Boyle and D. A. Dixon. 2008. The effects of initial conditions and liquid composition on the one-dimensional consolidation behaviour of clay-based sealing materials. Nuclear Waste Management Organization Report NWMO TR-2008-06.

RWE NUKEM Limited. 2003. Deep Geologic Repository: In-floor Borehole Emplacement – Design Changes from the In-room Emplacement Concept. Report No. 89125/REP/02. RWE NUKEM Limited.

Stroes-Gascoyne, S. and C.J. Hamon. 2008. The effect of intermediate dry densities (1.1-1.5 g/cm$^3$) and intermediate porewater salinities (60-90 g NaCl/L) on the culturability of heterotrophic aerobic bacteria in compacted 100% bentonite. Nuclear Waste Management Organization Technical Report NWMO TR-2008-11.

Weber, H.P. and M. Plötze. 2007. Emplacement tests with granular bentonite. In: Proceedings of Clays in Natural and Engineered Barriers for Radioactive Waste Confinement, 3rd International Meeting, Lille, France, p. 247.

# APPENDIX A: TWO MODEL VERIFICATION PROBLEMS

## CONTENTS

**Page**



## LIST OF FIGURES

**Page**

## A.1 LINEAR-ELASTIC AXISYMMETRIC TWO MATERIAL MODEL

A two-material linear-elastic axisymmetric model was implemented to verify the FLAC modelling approach by comparing numerical model results with the exact analytical solution for the same problem. Material properties and model geometries were arbitrarily selected. Poisson's Ratio used for the linear elastic analysis was 0.3. The situation modelled is illustrated in Figure A.1. The distance to the interface between the two materials was selected in order that the cross-sectional areas of the inner and outer rings were equal. The FLAC grid shown in Figure A.1 represented a 1 m thickness of the two ring model using FLAC's axisymmetric mode.

The swelling pressure was implemented by initializing it as a compressive stress in all FLAC zones and then subsequently allowing the material to expand or compress. The high swelling pressure material would expand and, as it did so, the mean stress would decrease. The low swelling pressure material, having a lower initial compressive stress, would decrease in volume resulting in an increase in mean stress. The two materials equilibrate when the radial stress in the inner material is equal to the radial stress in the outer material at the location where the two materials are in contact. The analytical solution for the problem was developed from the principles of linear-elasticity in concentric cylinders. The results from the analytical solution and the numerical model are provided in Figure A.2. The close agreement between the results indicated that the method of incorporating swelling pressure used in the user-defined FLAC subroutine was acceptable.

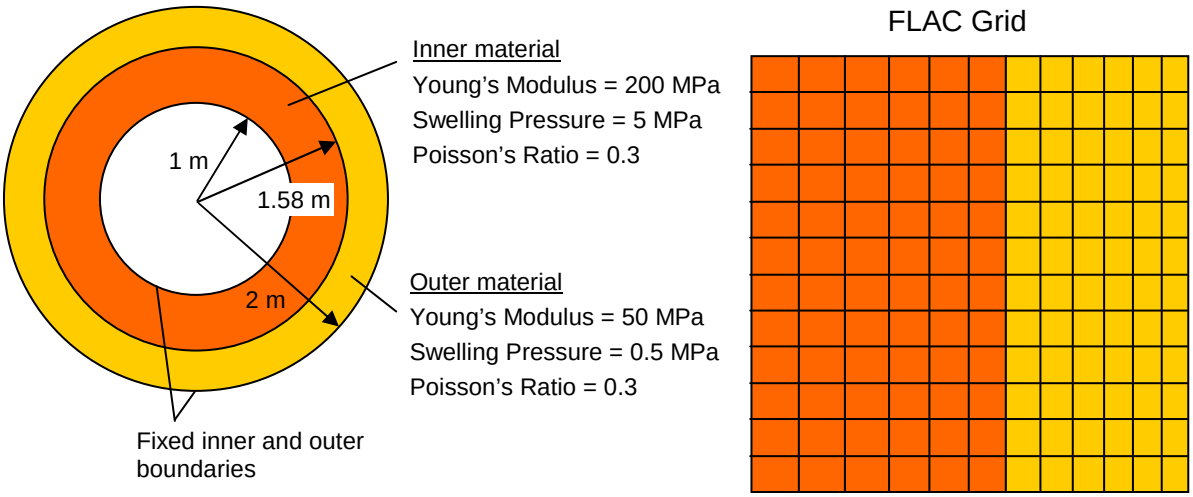


**Figure A.1: Axisymmetric Two-Material Linear-Elastic Model and FLAC Grid**

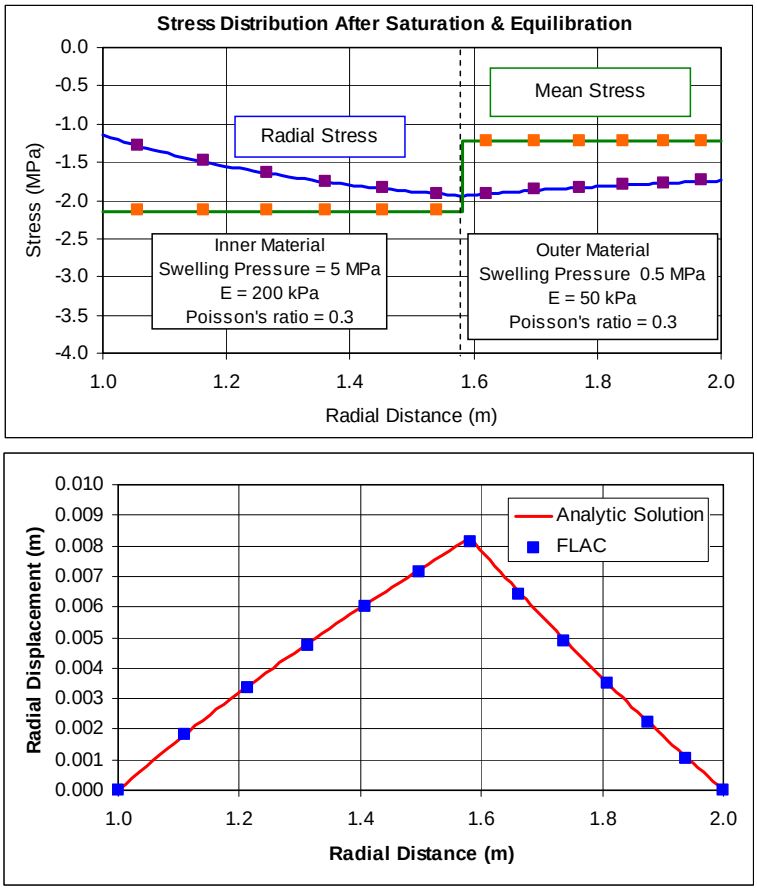


Radial and mean stress are shown in the upper plot, radial displacement is shown in the lower plot.

**Figure A.2: Comparison of Analytical Solution (Solid Lines) and FLAC Results (■) for the Verification Problem**

## A.2 STRAIN DEPENDENT BULK MODULUS WITH ONE MATERIAL

The second verification problem involved gradual free expansion of highly compacted bentonite (HCB). The analysis computed the change in vertical stress, radial stress and mean stress of a non-linear elastic material as a function of vertical displacement of the upper face of the clay specimen. The verification problem tested the ability of the FLAC model to produce mathematically acceptable solutions using Bulk and Shear Moduli that decreased with increasing strain. This analysis differed from the first verification problem that used constant Bulk and Shear Moduli. The HCB was constrained within a rigid walled cylinder with the top surface allowed to displace upwards by 7 mm for an initially 50 mm long specimen (Figure A.3). The HCB was assumed to be saturated immediately, although expansion was only gradually allowed with no imposed time scale. The initial vertical and lateral stresses were both assumed to be equal to the initial mean stress ($\sigma_{mo}$). The vertical and lateral stresses for the analytical solutions were defined using the following equations.

$$\sigma_{vertical} = \sigma_{mo} + \left(1 + \frac{2(1-2\upsilon)}{(1+\upsilon)}\right)(\sigma_{mo} - \sigma_{m})$$

$$\sigma_{lateral} = \sigma_{mo} + \left(1 - \frac{(1-2\upsilon)}{(1+\upsilon)}\right)(\sigma_{mo} - \sigma_{m})$$

where $\sigma_{mo}$ is the initial mean stress or swelling pressure and $\nu$ is Poisson's Ratio. The movement of the top plate of the FLAC model was sufficiently slow to allow the model to come into equilibrium as the top surface displaced. The modelled stresses as a function of vertical displacement of the upper surface is shown in Figure A.3. The analytical solution is very similar to the FLAC model results adding credibility to theoretical correctness of the non-linear FLAC model for volume expansion described in this report.

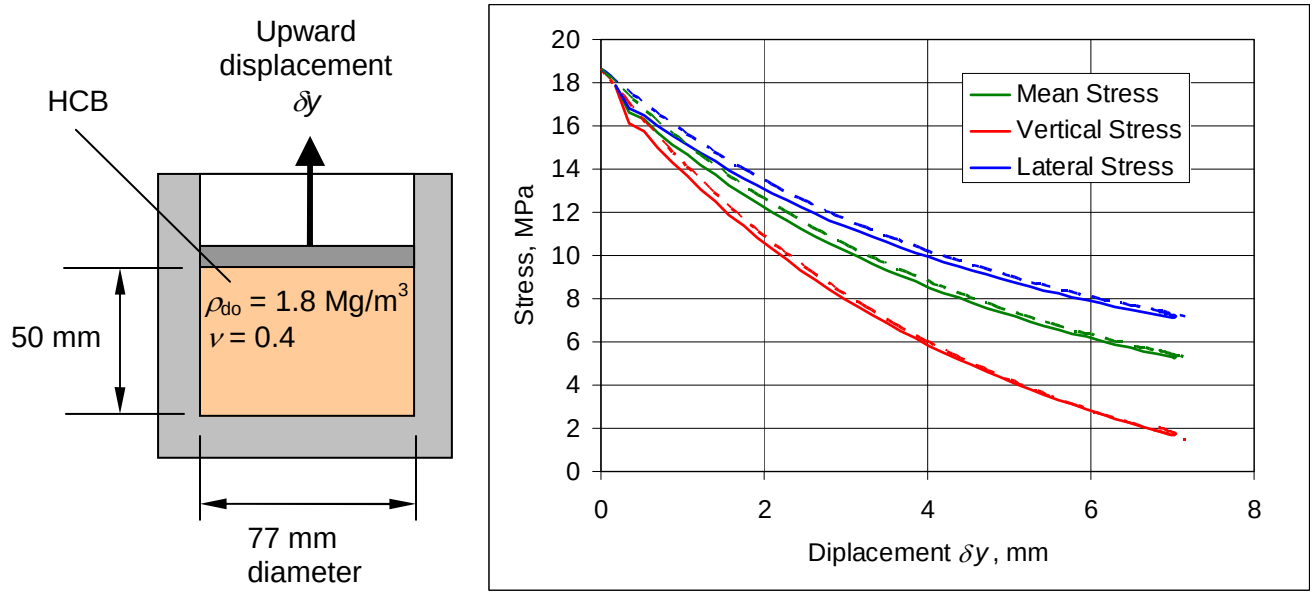


**Figure A.3: Volume Expansion Test of Modelled Results – the Solid Line is the FLAC model, the dashed line is the analytical solution.**

## APPENDIX B: PLOTS OF MEAN STRESS, DRY DENSITY AND EMDD NEAR THE CONTAINER SURFACE FOR THE HORIZONTAL PLACEMENT OPTION

## LIST OF FIGURES

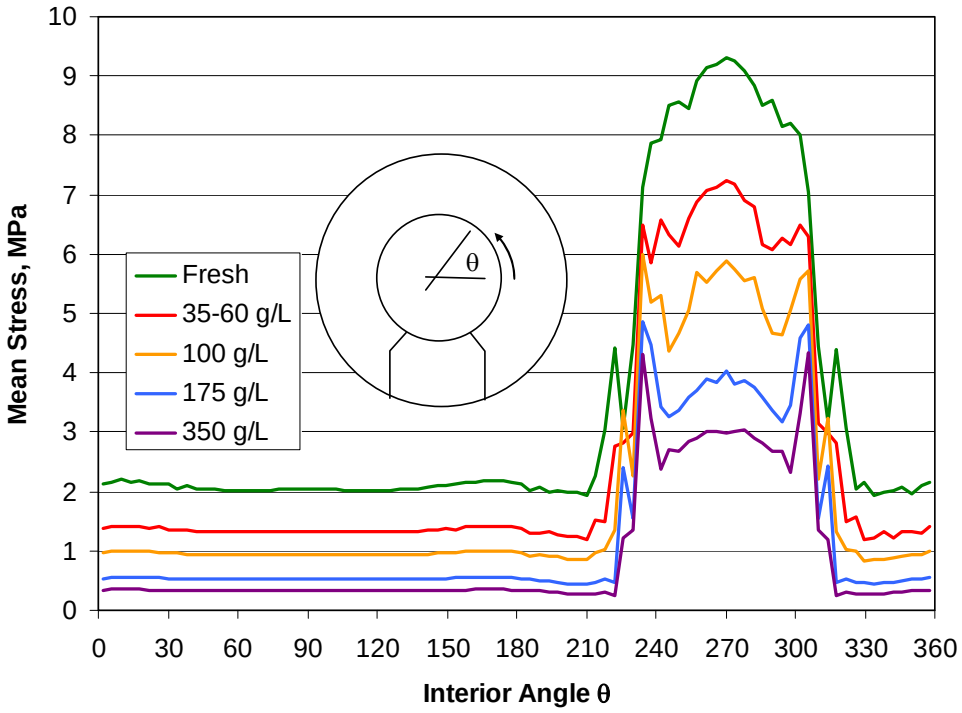


**Figure B.1: Mean Stress in the Bentonite Adjacent to the Container Surface for the Case of Initial Pellet Density of 1.35 Mg/m$^3$.**

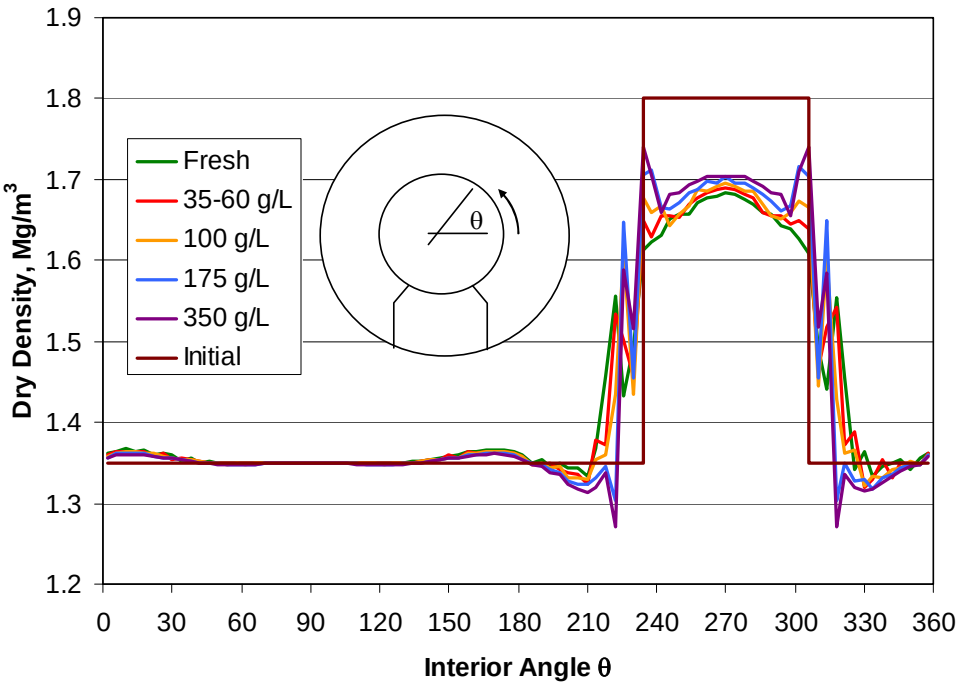


**Figure B.2: Dry Density of the Bentonite Adjacent to the Container Surface for the Case of Initial Pellet Density of 1.35 Mg/m$^3$.**

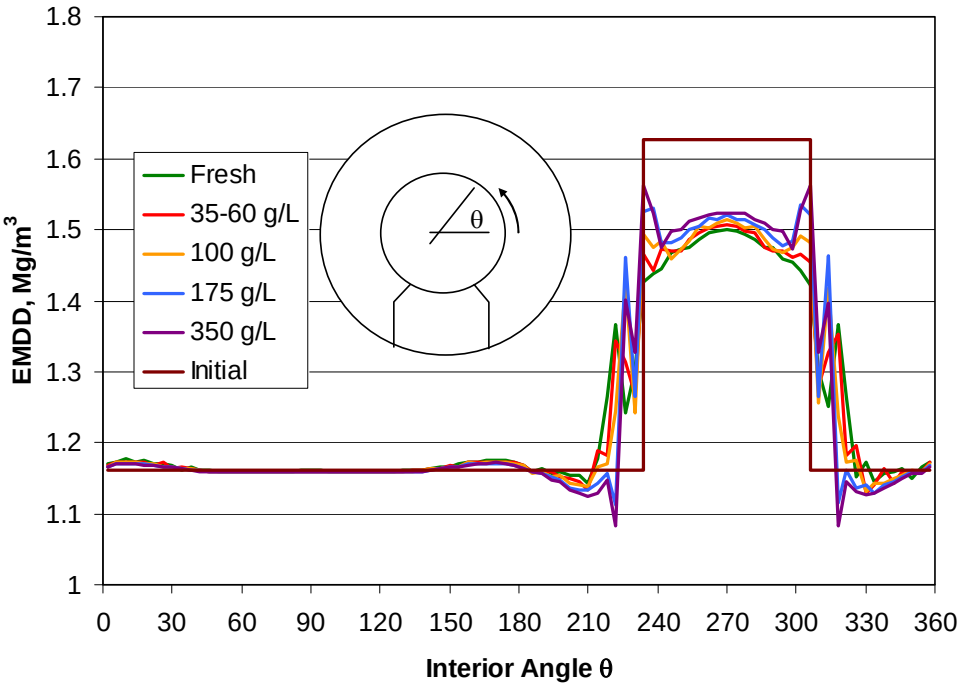


**Figure B.3: EMDD of the Bentonite Adjacent to the Container Surface for the Case of Initial Pellet Density of 1.35 Mg/m$^3$.**

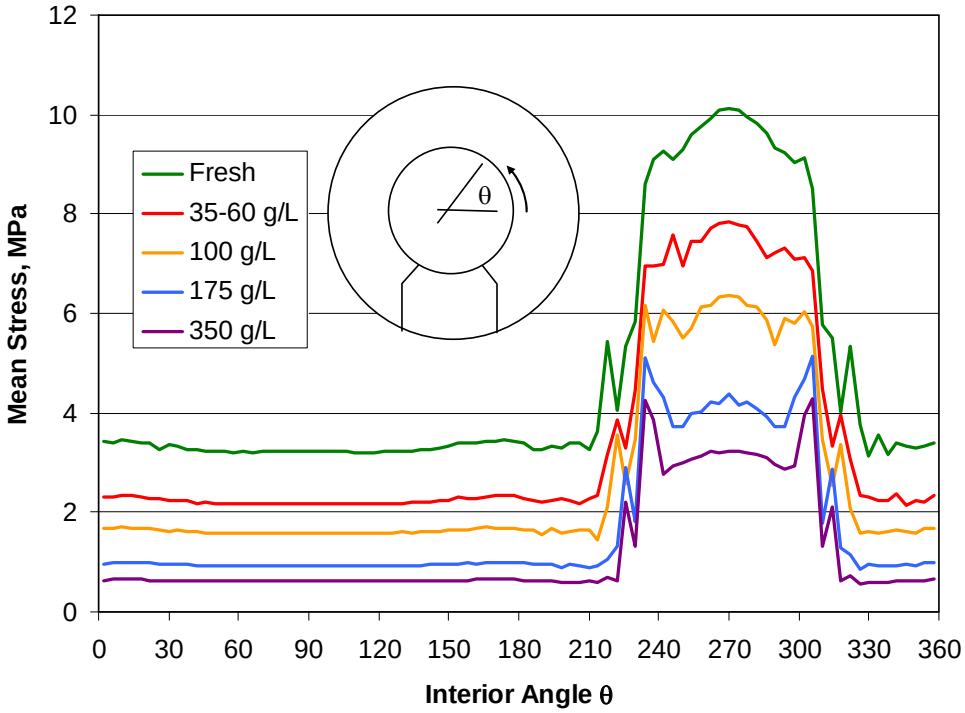


**Figure B.4: Mean Stress in the Bentonite Adjacent to the Container Surface for the Case of Initial Pellet Density of 1.45 Mg/m$^3$.**

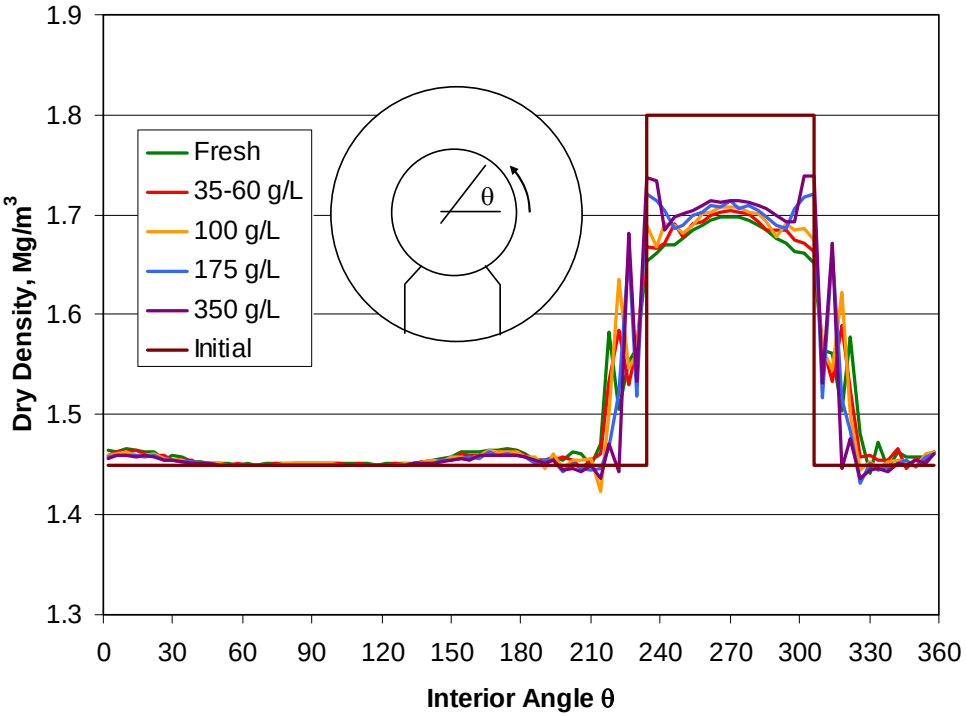


**Figure B.5: Dry Density of the Bentonite Adjacent to the Container Surface for the Case of Initial Pellet Density of 1.45 Mg/m$^3$.**

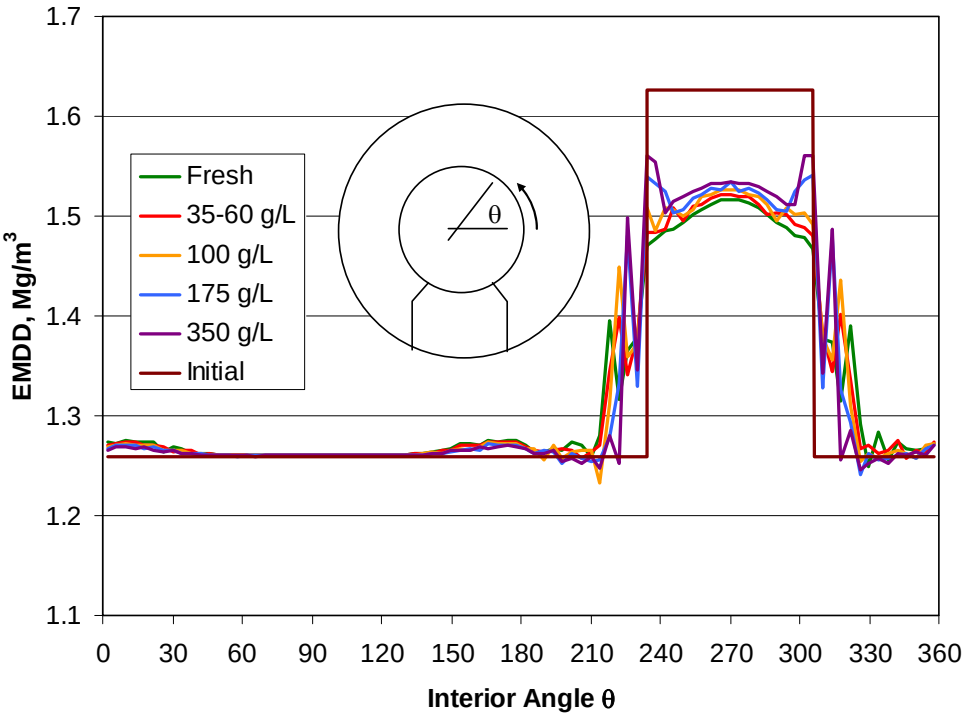


**Figure B.6: EMDD of the Bentonite Adjacent to the Container Surface for the Case of Initial Pellet Density of 1.45 Mg/m$^3$.**

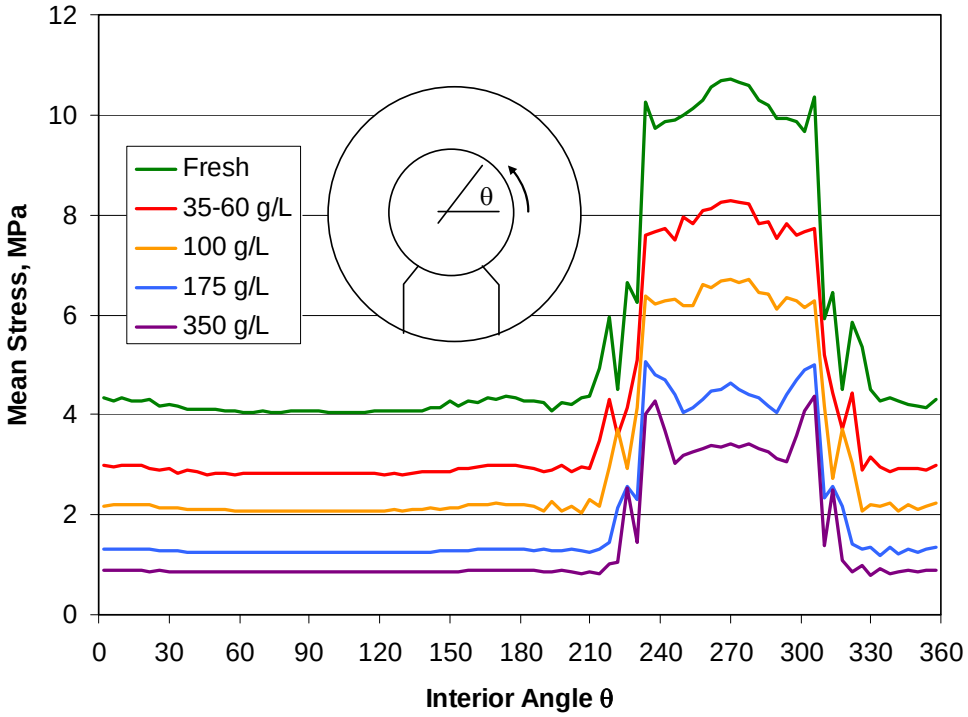


**Figure B.7: Mean Stress in the Bentonite Adjacent to the Container Surface for the Case of Initial Pellet Density of 1.50 Mg/m$^3$.**

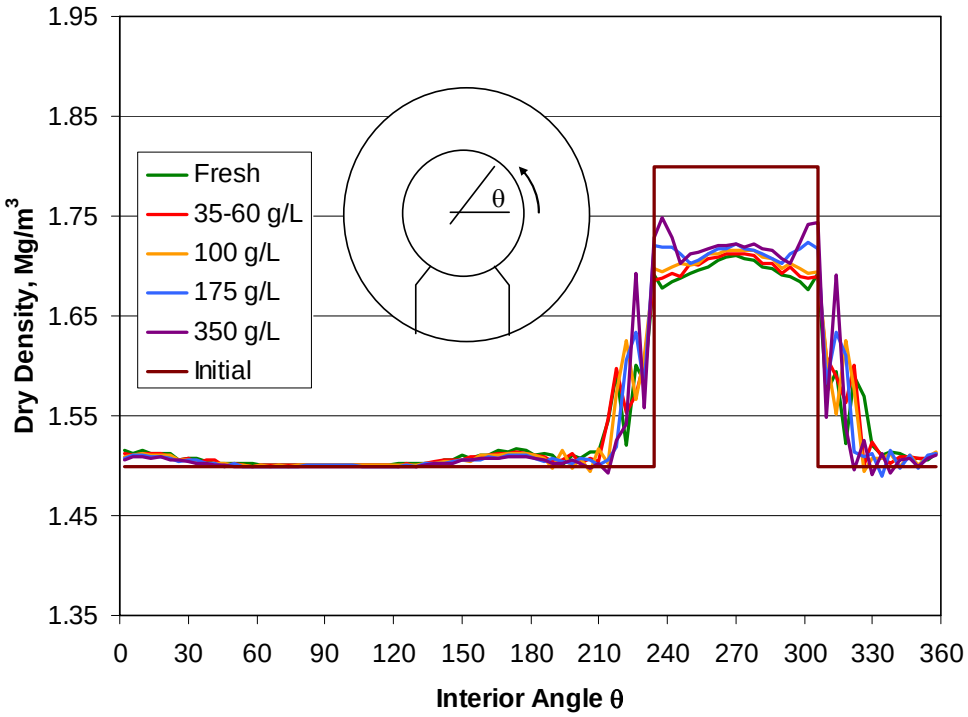


**Figure B.8: Dry Density of the Bentonite Adjacent to the Container Surface for the Case of Initial Pellet Density of 1.50 Mg/m$^3$.**

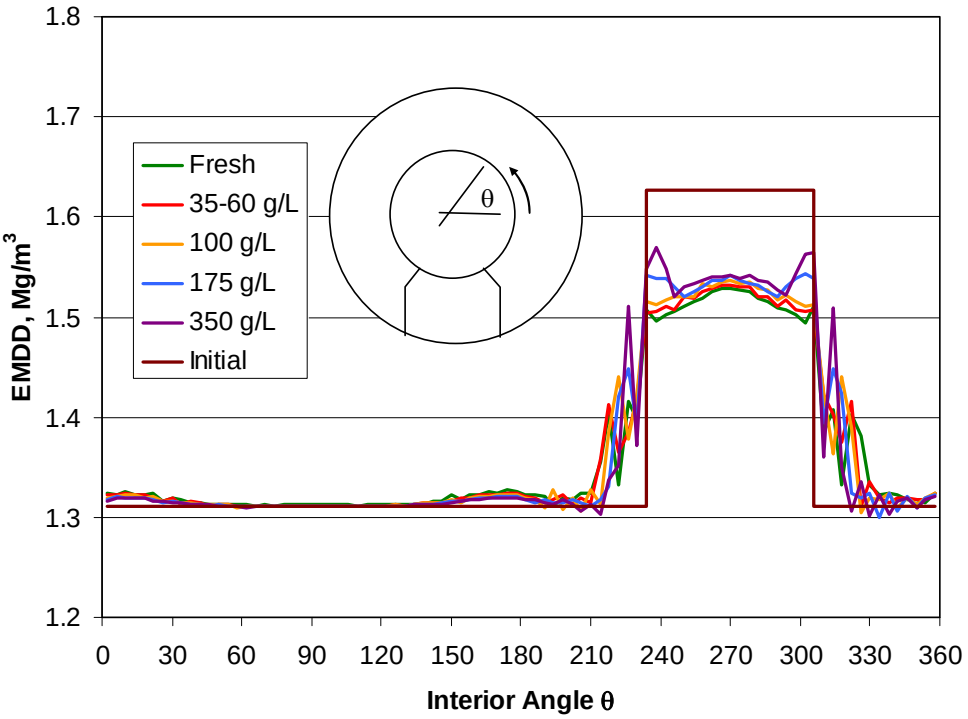


**Figure B.9: EMDD of the Bentonite Adjacent to the Container Surface for the Case of Initial Pellet Density of 1.50 Mg/m$^3$.**